Increases in cyclin A/Cdk activity and in PP2A-B55 inhibition by FAM122A are key mitosis-inducing events

Benjamin Lacroix, Suzanne Vigneron, Jean Claude Labbé, Lionel Pintard, Corinne Lionne, Gilles Labesse, Anna Castro, Thierry Lorca

Increases in cyclin A/Cdk activity and in PP2A-B55 inhibition by FAM122A are key mitosis-inducing events

Benjamin Lacroix[1,4*], Suzanne Vigneron[1,4*], Jean Claude Labbé[1,4], Lionel Pintard[2,4], Corinne Lionne[3], Gilles Labesse[3], Anna Castro[1,4&] and Thierry Lorca[1,4&]

[1]Université de Montpellier, Centre de Recherche en Biologie cellulaire de Montpellier (CRBM), CNRS UMR 5237, 1919 Route de Mende, 34293 Montpellier cedex 5, France.

[2]Université Paris Cité, Institut Jacques Monod, F-75013 Paris,France.

[3]Centre de Biochimie Structurale (CBS), CNRS UMR 5048, INSERM 1054, Université de Montpellier, Montpellier, France.

[4]Programme équipes Labellisées Ligue Contre le Cancer

Phone 33 4 34 35 95 56

Fax 33 4 34 35 94 10

[*]Both authors contributed equally to this work

[&]Corresponding authors: thierry.lorca@crbm.cnrs.fr / anna.castro@crbm.cnrs.fr

ABSTRACT

Entry into mitosis has been classically attributed to activation of a cyclin B/Cdk1 amplification loop via a partial pool of this kinase becoming active at the end of G2 phase. However, how this initial pool is activated is still unknown. Here we discovered a new role of the recently identified PP2A-B55 inhibitor FAM122A in triggering mitotic entry. Accordingly, depletion of the orthologue of FAM122A in *C. elegans* prevents entry into mitosis in germline stem cells. Moreover, data from *Xenopus* egg extracts strongly suggest that FAM122A-dependent inhibition of PP2A-B55 could be the initial event promoting mitotic entry. Inhibition of this phosphatase allows subsequent phosphorylation of early mitotic substrates by cyclin A/Cdk, resulting in full cyclin B/Cdk1 and Greatwall (Gwl) kinase activation. Subsequent to Greatwall activation, Arpp19/ENSA become phosphorylated and now compete with FAM122A, promoting its dissociation from PP2A-B55 and taking over its phosphatase inhibition role until the end of mitosis.

Keywords: FAM122A, Arpp19, PP2A-B55, mitosis, Cyclin A.

INTRODUCTION

Mitotic entry and progression are induced by massive protein phosphorylation resulting from the fine-tuned balance between the kinase cyclin B/Cdk1 and its counteracting phosphatase PP2A-B55(Mochida *et al*, 2010; Gharbi-Ayachi *et al*, 2010; Mochida *et al*, 2009; Vigneron *et al*, 2009). Cyclin B/Cdk1 activity is maintained low during G2 by the Wee1/Myt1 kinases that phosphorylate Cdk1 on its inhibitory site tyrosine 15. At M phase entry, cyclin B/Cdk1 activity is triggered by a positive feed-back loop(Pomerening *et al*, 2003; Sha *et al*, 2003). A partial active pool of this kinase phosphorylates Wee1/Myt1, as well as the Cdc25 phosphatase responsible of Cdk1-tyrosine 15 dephosphorylation, promoting a rapid and complete activation of the cyclin B/Cdk1 complex. How cyclin B/Cdk1 partial activation is firstly triggered at G2-M is a main question yet to be answered. Inhibition of PP2A-B55 was proposed as the putative cause inducing partial cyclin B/Cdk1 pool activation and mitotic entry. PP2A-B55 is regulated by the Gwl-Arpp19/ENSA pathway(Mochida *et al*, 2010; Gharbi-Ayachi *et al*, 2010; Burgess *et al*, 2010; Hached *et al*, 2019). During G2, the activity of this phosphatase is high. Then, at mitotic entry, Gwl is activated and phosphorylates its substrates Arpp19/ENSA converting them into high affinity inhibitors of PP2A-B55. Decreased PP2A-B55 activity could then favour a partial Wee1/Myt1/Cdc25 phosphorylation and reactivation of cyclin B/Cdk1 triggering the feedback loop. However,

Gwl activation itself depends on cyclin B/Cdk1 discarding the modulation of this phosphatase by the Gwl-Arpp19/ENSA pathway as the first event triggering cyclin B/Cdk1 firing and mitotic entry(Vigneron *et al*, 2011; Blake-Hodek *et al*, 2012). Moreover, although both Gwl and Arpp19/ENSA are essential for mitotic entry in *Xenopus* egg extract model(Gharbi-Ayachi *et al*, 2010; Vigneron *et al*, 2009), the depletion of these proteins do not prevent G2-M transition in human and mouse cells(Hached *et al*, 2019; Alvarez-Fernandez *et al*, 2013).

Besides cyclin B/Cdk1, cyclin A/Cdk is also present and is a poor substrate of Myt1 kinase during G2(Coulonval *et al*, 2003; Booher *et al*, 1997). This kinase could participate to Wee1/Myt1/Cdc25 phosphorylation during G2-M if the activity of PP2A-B55 is partially inhibit during this transition. In this line, FAM122A has been recently described as a new inhibitor of PP2A-B55 that is present and active during G2.

FAM122A was firstly identified as an interactor of the PP2A-B55 complex that inhibits this phosphatase and promotes the degradation of PP2A catalytic subunit.(Fan *et al*, 2016) This protein was additionally shown to negatively modulate PP2A-B55α in the nucleus. Its phosphorylation by Chk1 and its subsequent retention into the cytoplasm is essential for the G2/M checkpoint by preventing the nuclear inhibition of this phosphatase and permitting the dephosphorylation and stabilisation of Wee1(Li *et al*, 2020). By its presence in G2 and its capacity to specifically inhibit PP2A-B55, FAM122A is a good candidate to fulfil the role of PP2A-B55 inhibitor able to potentiate cyclin A/Cdk-dependent phosphorylation at G2 and to trigger M phase. In this study we investigated the role of FAM122A in mitotic entry and we demonstrated that, by inhibiting PP2A-B55, this protein promotes a first burst of cyclin A/Cdk-dependent phosphorylation that will induce cyclin B/Cdk1 activation and mitotic entry.

RESULTS

PP2A-B55 inhibition by FAM122A does not involve changes in PP2A-C or Wee1 levels

The role of FAM122A as a specific PP2A-B55 inhibitor has been reported by two different laboratories(Fan *et al*, 2016; Li *et al*, 2020). One laboratory reported a role of this protein in the negative modulation of PP2A-B55 via the degradation of the PP2A-B55 catalytic subunit C(Fan *et al*, 2016). The second one suggested that the inhibition of PP2A-B55 by FAM122A induces the dephosphorylation and degradation of Wee1. We checked these two premises in interphase *Xenopus* egg extracts (interphase extracts), in which protein phosphorylation mimics the one observed in G2 cells. We, therefore, added either *Xenopus* or

human histidine recombinant FAM122A proteins to these extracts and measured the levels of PP2A-C and Wee1 over time. Surprisingly, we could not observe any variation of the amount of these two proteins in the extracts (Figure 1a). We next proceeded by checking whether our recombinant FAM122A forms can inhibit PP2A-B55. To do this, we used interphase egg extracts in which ATP was eliminated and thus endogenous kinases are inactive (called hereafter as kinase-inactivated extracts). Because of the absence of endogenous active kinases, substrate dephosphorylation in these extracts directly reflects phosphatase activity(ies). Kinase-inactivated extracts were supplemented, or not, with the corresponding FAM122A recombinant protein (human/*Xenopus*) and subsequently with recombinant Arpp19 pre-phosphorylated at S113 by PKA known to be a bona fide PP2A-B55 substrate(Labbé *et al,* 2021; Lemonnier *et al,* 2019). Dephosphorylation of S113 of Arpp19 was then followed by western blot over time. As expected by its capacity to inhibit PP2A-B55, both human and *Xenopus* FAM122A drastically delayed Arpp19 dephosphorylation (Figure 1b). Similar results were observed using phosphorylated-T481 PRC1, another well-established substrate of PP2A-B55 phosphatase(Cundell *et al,* 2013). We next checked the association of His-FAM122A to PP2A-B55 by using histidine-pull down. B55, A and C subunits of PP2A were present in the histidine but not in the control pull-down of *Xenopus* and human FAM122A (Figure 1c). Thus, FAM122A can directly bind and inhibit PP2A-B55 without any modification of the levels of the catalytic subunit of this phosphatase.

FAM122A triggers mitotic entry by inhibiting PP2A-B55 and permitting cyclin A/Cdk-dependent phosphorylation of mitotic substrates

We next checked the impact of FAM112A on mitotic progression by measuring the phosphorylation of mitotic substrates upon the addition of this protein into interphase extracts. FAM122A induced a first phosphorylation of Gwl, the Anaphase Promoting Complex (APC) subunit Cdc27, and of Cdc25 concomitantly with the activation of cyclin B/Cdk1 as reflected by the loss of the phosphate on tyrosine 15 inhibitory site of Cdk1. This was followed by the subsequent degradation of cyclin A and B and the dephosphorylation of the above indicated substrates revealing that FAM122A promotes mitotic entry but is unable to maintain the mitotic state (Figure 2a). We then sought to assess whether, as for Arpp19, FAM122A requires phosphorylation by Gwl to stably bind and inhibit PP2A-B55. Against this hypothesis, our data indicate that Gwl is unable to phosphorylate FAM122A "*in vitro*" (Figure 2b) and the depletion of this kinase in interphase extracts did not prevent mitotic entry induced by FAM122A (Figure 2c). Moreover, a FAM122A form in which all serine and

threonine residues were mutated into alanine kept its capacity to induce mitosis (S/T-A FAM122A, Figure 2d) and displayed a similar PP2A-B55 binding capacity than the wildtype FAM122A (Figure 2e). These data suggest that FAM122A phosphorylation is not required for its binding to and the inhibition of PP2A-B55 at least at the used ectopic doses although we cannot exclude other PP2A-B55-independent role of this phosphorylation. Thus, FAM122A would not require either phosphorylation or Gwl activity to trigger mitotic entry.

We then investigated whether mitotic substrate phosphorylation induced by FAM122A requires cyclin B/Cdk1 activation by examining the effect of depleting Cdc25, the phosphatase dephosphorylating tyrosine 15 of Cdk1 and triggering cyclin B/Cdk1 activity. As expected, Cdc25-devoid extracts displayed inactive cyclin B/Cdk1, as stated by the presence of the phospho-tyrosine 15 on Cdk1 (Figure 2f). Moreover, cyclin A became fully proteolyzed whereas cyclin B remained mostly stable although we detected a loss of a small fraction of this protein likely due to the phosphorylation, under these conditions, of Cdc27 and the activation of the APC. Besides Cdc27, FAM122A, via PP2A-B55 inhibition, was also able to promote the phosphorylation and activation of Gwl and, most importantly, the phosphorylation and inactivation of the Cdk1 inhibitory kinase Myt1. Since due to Cdc25 depletion cyclin B/Cdk1 was inactive in these extracts, we attributed these phosphorylations to cyclin A/Cdk1. In this line, we previously showed that this complex escapes to Wee1-Myt1 inhibitory phosphorylation and is fully active in interphase extracts (Vigneron *et al,* 2018). To confirm this hypothesis, we co-depleted Cdc25 and cyclin A in FAM122A-supplemented interphase extracts. Remarkably, the loss of these two proteins prevented substrate phosphorylation resulting from FAM122A-dependent inhibition of PP2A-B55 (Figure 2f). However, this phosphorylation was restored again if 45 minutes upon Cdc25/cyclin A co-depletion and FAM122A addition, cyclin A was supplemented again to these extracts. These data demonstrate that the decrease of the PP2A-B55 activity in interphase extracts induced by FAM122A is sufficient to permit cyclin A-Cdk1-dependent phosphorylation that will then trigger cyclin B/Cdk1 reactivation. Interestingly, this suggests that an increase of the endogenous levels of either FAM122A or cyclin A would be sufficient to trigger mitotic entry and would thus escape to the negative regulation of active PP2A-B55 during interphase.

Molecular determinants of FAM122A controlling the association and the inhibition of PP2A-B55

AlphaFold artificial intelligence software (Alphabet's/Google's DeepMind) predicts the presence of two αhelices in the FAM122A protein, α-helix1: residues 84-93 (human)/71-

82 (*Xenopus*) and α-helix2: residues 96-119 (human)/85-110 (*Xenopus*) (Figure 3a). In order to investigate if these structured regions could participate to the association of this protein to PP2A-B55, we constructed a FAM122A *Xenopus* mutant forms deleted of either α-helix1 (αH1) or α-helix2 (αH2) and we measured their capacity to induce mitotic entry and to bind to PP2A B55 and C subunits when added to interphase extracts. Neither of these two mutants were able to induce mitosis (Figure 3b) or to bind to PP2A-B55 (Figure 3c) indicating that these two regions are essential for FAM122A inhibitory activity. We next constructed a N-terminal Δ(1-72) and a C-terminal (Δ110-270) mutant forms in order to determine whether any of these regions could additionally participate to the functionality of this protein. Unlike the two α-helix regions, these two mutants displayed similar properties than the wildtype form (Figure 3d and e). Finally, we proceed with the construction of FAM122A single mutant forms for all conserved residues present in αH1 and αH2 regions. Data on mitotic entry and PP2A-B55 binding capacities of these mutants are shown in Appendix Figure S1a and S1b and summarized in Figure 3f. Residues of αH1, R73, L74, I77 and E80 were essential for FAM122A inhibitory activity. Indeed, αH1 sequence SRLHQIKQEE, is close to the previous reported Short Linear Motif (SLiM) designed for PP2A-B55, with consensus sequence p[ST]-P-x(4,10)-[RK]-V-xx-[VI]-R(Fowle *et al,* 2021) and is highly conserved between species (Appendix Figure S1c). This motif is present in PP2A-B55 substrates and is required for their binding to the phosphatase via their interaction with the B55 subunit. As so, these residues are involved in FAM122A association to B55. For αH2 region, we identified positions E90, H93, E94 and R95 as being essential for FAM122A activity. Thus, we pinpointed these two structured regions of FAM122A essential for its function and we identified the key residues directly mediating PP2A-B55 phosphatase interaction.

Gwl activation at mitotic entry promotes the dissociation of FAM122A from PP2A-B55

Data above demonstrate that the addition of FAM122A to interphase extracts promotes mitotic entry but is unable to maintain mitotic substrate phosphorylation. Since the levels of FAM122A remain constant throughout the experiment and that FAM122A activity appears not to be impacted by phosphorylation, we sought to understand why FAM122A is not able to maintain the mitotic state. To this, we first checked the capacity of *Xenopus* and human FAM122A proteins to bind PP2A-B55 when they were supplemented to metaphase II arrested extracts (CSF extracts) which mimics the mitotic state. Interestingly, B55 and C subunit binding to FAM122A is clearly observed during interphase, whereas no association

for B55 and a drastic decrease for C catalytic subunit were observed in CSF extracts (Figure 4a).

To corroborate these observations, we tested whether FAM122A would be dissociated from B55 subunit in extracts blocked in mitosis. In order to obtain mitotic blocked extracts, we prevented cyclin B degradation in interphase extracts by the depletion of the APC subunit Cdc27 and then we added FAM122A. FAM122A addition promoted mitotic entry but, because of the incapacity to proteolyze cyclin B, extracts remained blocked in this phase of the cell cycle. Under these conditions, we measured the temporal pattern of protein phosphorylation and association of FAM122A to PP2A-B55. As expected, addition of FAM122A to control interphase extracts promoted mitotic entry and exit, while mitosis was maintained throughout the experiment when Cdc27 was depleted (Figure 4b). In control extracts, FAM122A rapidly associated to B55, A and C subunits from its addition, then dissociated concomitantly with mitotic entry and re-associated again upon exit of mitosis by cyclin B degradation (Figure 4b). Conversely, in Cdc27-depleted interphase extracts, FAM122A also displayed a first association to these proteins but then, definitively lost this interaction from the establishment of the mitotic state. Taken together, these observations suggest that FAM122A-B55 binding is prevented during mitosis.

Besides, cyclin B/Cdk1, the Gwl kinase is also required to maintain the mitotic state. Although our data shown above demonstrate that Gwl cannot phosphorylate FAM122A to promote mitotic entry, we tested whether the PP2A-B55 inhibitory activity of FAM122A could be indirectly modulated by this kinase once the mitotic state is achieved. To this, we repeated the previous experiment except that extracts were immunodepleted of both, Cdc27 and the Gwl kinase. As expected by the depletion of Cdc27, all extracts entered into mitosis and kept the mitotic state as shown by the stability of cyclin B, the continuous phosphorylation of Cdc25 and the loss of phospho-tyrosine 15 Cdk1 signal throughout the experiment (Figure 4c). Interestingly, unlike Cdc27/control-co-depleted extracts (Figure 4c, lane 1, His Pull Down) and despite the presence of a fully active cyclin B/Cdk1 complex, FAM122A was able to bind to B55 and to increase its association to PP2A C subunit in Cdc27/Gwl-co-depleted extracts (Figure 4c, lane 2, His Pull Down). However, FAM122A dissociated again from B55 when a Gwl hyperactive form was further supplemented (Figure 4c, lane 4, His Pull Down). Thus, FAM122A dissociation from PP2A during mitosis is modulated by the Gwl kinase.

Arpp19 competes and dissociates FAM122A from PP2A-B55 during mitosis

We next sought to decipher how Gwl could regulate FAM122A association to PP2A-B55. Gwl phosphorylates Arpp19 during mitosis, turning it into a high affinity interactor of PP2A-B55 (Mochida *et al*, 2010; Gharbi-Ayachi *et al*, 2010; Williams *et al*, 2014). We thus, asked whether during mitosis, phosphorylated Arpp19 competes with FAM122A for PP2A-B55 binding. To test this hypothesis, we supplemented interphase extracts with FAM122A and 40 minutes later, once the extract returned to an interphase state and FAM122A binds again PP2A-B55 (Figure 2a and 4b), it was either (1) used to perform a histidine-FAM122A pulldown and subsequently supplemented with thio-S71-phosphorylated Arpp19 or the other way around, (2) first supplemented with a thio-S71-phosphorylated Arpp19 and subsequently submitted to histidine-FAM122A pulldown (Figure 5a, scheme). Finally, FAM122A association to B55 was measured. Strikingly, the presence of a thio-S71-phosphorylated form of Arpp19 (Thio-S71-Arpp19) that cannot be dephosphorylated, induced the dissociation of FAM122A from PP2A-B55 in both cases confirming our hypothesis that Arpp19 displaces FAM122A from PP2A-B55 by competing for this phosphatase.

We also performed the reverse experiment and tested whether GST-FAM122A could dissociate a p-S71-Arpp19 complexed to PP2A-B55 phosphatase. Thus, CSF extracts were supplemented with His-Arpp19 protein. Because of the activated Gwl kinase present in these extracts, exogenous Arpp19 is immediately phosphorylated and tightly binds PP2A-B55. p-S71-Arpp19-PP2A-B55 complex was then recovered by histidine-pulldown and supplemented with high doses of GST-FAM122A. Then the level of B55 bound to pArpp19 was measured by western blot. Interestingly, the levels of B55 bound to pArpp19 did not change upon FAM122A addition indicating that FAM122A was unable to dissociate this protein from PP2A-B55 complex (Figure 5b). These data indicate that p-S71-Arpp19 has a much higher affinity for PP2A-B55 than FAM122A and induces its dissociation. Supporting this hypothesis, our data above (Figure 4 and Figure 5b) demonstrate that endogenous Arpp19 is able to dissociate ectopic His-FAM122A protein from PP2A-B55 despite we estimated the molarity of the former in these experiments being 215 times lower than the latter (0.1 µM endogenous Arpp19 versus 21.5 µM ectopic His-FAM122A, Appendix Figure S2a and S2b).

To deeper address the different binding affinities of pArpp19 and FAM122A for PP2A-B55, we performed kinetic studies directed to identify the inhibitor constants (K_i) of these two proteins by measuring dephosphorylation of p-S113-Arpp19 in kinase inactivated extracts supplemented with increasing doses of Thio-S71-Arpp19 or FAM122A. Inhibition of PP2A-B55 by FAM122A and Thio-S71-Arpp19 was characterized by varying both the

concentration of the substrate p-S113-Arpp19 (from 120 to 2000 nM) and that of the inhibitors FAM122A (from 0 to 250 nM) or Thio-S71-Arpp19 (from 0 to 3 nM). Of the four inhibition modes tested, the competitive mode was the one fitting the experimental data with the lowest reduced Chi^2 value which reflects the fitting quality (Appendix Figure S3 and S4). The values of the K_i were 28±4.6 nM for FAM122A and 0.22±0.04 nM for Thio-S-71-Arpp19 with a consistent Km for p-S113-Arpp19 of around 146±23.9 nM in both series of experiments (Figure 5c and Appendix Figures S3 and S4). The K_i for FAM122A was 127-fold higher than the one observed for Thio-S71-Arpp19, an affinity value very close to the one that we obtained by measuring p-S71-Arpp19-dependent dissociation of FAM122A in pulldown assays (215-fold higher). Thus, these data confirm the higher affinity of p-S71-Arpp19 for PP2A-B55 and its capacity to dissociate FAM122A of this phosphatase.

We next checked whether the temporal patterns of (1) association and dissociation of FAM122A/PP2A-B55, (2) activation of Gwl and (3) Gwl-dependent phosphorylation of Arpp19 in S71 conferring its PP2A-B55 inhibitory activity, were in line with the differential K_i constants obtained for FAM122A and Thio-S71-Arpp19. Accordingly, the addition of FAM122A to interphase extracts promoted the immediate presence of B55 in FAM122A pulldowns (10 minutes) and its subsequent dissociation concomitantly with Gwl activation (10 and 20 minutes) and Arpp19 phosphorylation (20 and 30 minutes) (Figure 5d). However, this protein was re-associated again once cyclin B was degraded, Gwl was inactivated and Arpp19 was dephosphorylated at mitotic exit (40 minutes). These data support that Arpp19 phosphorylation during mitosis promotes the dissociation of FAM122A from PP2A-B55 and takes over the inhibition of this phosphatase. However, to fully confirm the physiological role of FAM122A in mitotic entry, it is essential to show that ectopic FAM122A doses supplemented to these extracts are close to the endogenous concentration of this inhibitor. We thus tried to measure the endogenous concentration of FAM122A in *Xenopus* extracts. However, unfortunately, although our antibodies recognize the ectopic protein, they were unable to detect FAM122A in the extracts. Since this protein is nuclear (Li *et al*, 2020), we reasoned that it was lost during the purification of oocyte cytoplasmic fraction. As an alternative, we decided to compare the minimal dose of FAM122A used in the extracts to the concentration of endogenous FAM122A in human cells. By comparing western blot signals of recombinant His-FAM122A and RPE1 cell lysates we estimated endogenous FAM122A concentration to be 59.6 ± 6.37 nM (Appendix Figure S5). We next performed dose-response assays to identify the minimal dose of FAM122A inducing mitotic entry when supplemented

to interphase extracts using the wildtype and the phosphorylation S/T-A mutant FAM122A forms. We could establish that a dose between 3 and 15 nM of ectopic wildtype FAM122A was sufficient to promote mitotic entry (Figure 5e). Conversely, the S/T-A FAM122A mutant minimal dose inducing mitotic entry was fixed between 30 and 75 nM suggesting that the phosphorylation of this protein exerts a positive role, but is not essential for PP2A-B55 inhibition. Moreover, although higher than the one obtained for the wildtype protein, S/T-A FAM122A mutant minimal concentration is very close to the one estimated for endogenous FAM122A in human cells (30 to 75 vs 59.6 nM). All together these data are in line with a first role of FAM122A in PP2A-B55 inhibition at mitotic entry that would be subsequently taken over by Arpp19 once phosphorylated by active Gwl.

The different binding of Arpp19 and FAM122A to PP2A-B55 could explain the ability of the first inhibitor to dissociate the second from phosphatase

In order to understand how Arpp19 can dissociate FAM122A from PP2A-B55, we modeled the quaternary complex of PP2A with Arpp19 from three distant species (human, *Xenopus* and *C. elegans*) using Alphafold_multimer (preprint: Evans *et al*, 2021) with default settings and no relaxation. The resulting models looks globally similar. The molecular organization of the PP2A subunits reproduces well the known crystal structure (PDB3DW8) with little unfolded regions. Arpp19 (for the human and *Xenopus* complexes) and the unique orthologue for Arpp19/ENSA in *C. elegans* called ENSA are mostly unfolded (Figure 6a, left panel, orange) and share three common helical stretches, labelled hereafter as α1, α2 and α3. A first helix, α0, in human Arpp19 and *Xenopus* Arpp19, that is not predicted in worm ENSA, seems to form no interaction with PP2A and will not be further considered. On the contrary, the three conserved helices (α1: residues 24-35, α2 :45-54 and α3 :60-73 in human Arpp19) are predicted to interact with the phosphatase. The first two contact the B55 subunit (Figure 6a, left panel, blue) while the third one points toward the catalytic site of the C subunit (Figure 6a, left panel, green). No contact is detected between the Arpp19 chains with the scaffolding subunit (Figure 6a, left panel, violet). The interaction with B55 mainly relies on the helix α1 that displays tight contacts along the helix from Arpp19. The interactions conserved among the three complexes includes two salt bridges (E25 and R35 from Arpp19 with R330 and E338 from B55 in the human complex) and hydrophobic interactions involving L32 from Arpp19 and F280, F281 and C334 from B55 subunit in human. In addition, two N-capping and one C-capping (involving E28, E29 and K26 in human and

Arpp19, respectively) are predicted. The second helix of Arpp19, α2, shows more loose interactions and it seems to mainly bridge the helix α1 with the third helix. Helix α3 partially overlaps with the QKYFDSGDY motif conserved in all Arpp19 and ENSA sequences and containing the serine phosphorylated by Gwl. This phosphorylation is essential for strong inhibition of PP2A. We modeled the phosphoserine using a dedicated server (https://isptm2.cbs.cnrs.fr described in the "Methods" section) and also added the two manganese atoms within the catalytic center of the C subunit of PP2A for further analysis. Although in the human and *Xenopus* complexes, the serine is not predicted to directly interact with the catalytic manganese (distance PO4-Mn: ~ 8 A), such interactions appeared plausible in the worm complex (distance PO4-Mn: ~ 5 A). This direct contact would explain the strong interaction of phosphorylated Arpp19 with PP2A-B55, although it is worth highlighting that the Mn^{2+} ion present in the structure obtained with recombinant PP2A-B55 enzyme does not correspond to the Zn^{2+}:Fe^{2+} divalent cation pair known to be present in the native PP2A-B55 enzyme (Brautigan & Shenolikar, 2018). However, the inhibitory activity has been shown to be not only characterized by the high affinity of Arpp19 towards PP2A-B55, but also by the slow dephosphorylation of its Gwl site (Labbé *et al*, 2021). The present modeling does not permit to fully understand the absence of catalytic activity on the phosphorylated serine. However, this model agrees with the previously reported mutational scanning of the QKYFDSGDY motif (Labbé *et al*, 2021) to suggest that a precise and peculiar orientation of the phosphorylated sidechain would be required to maintain a tight but unreactive interaction. Indeed, mutations to alanine of close phosphoserine neighbor residues in this sequence dramatically accelerate Arpp19 dephosphorylation by PP2A-B55 while lowering binding at the same time (Labbé *et al*, 2021; Williams *et al*, 2014). Additional interactions are predicted at this interface in the worm complex (and partially reproduced in the human and *Xenopus* assemblies) (see Figure 6b). These interactions include two salt-bridges involving the Gwl site phosphoserine (S62) and the preceding aspartate residue (D61) from human Arpp19 and two arginines of human PP2A C subunit (R89 and R214) lying at the entrance of the catalytic site. Another salt bridge may occur between another aspartate from Arpp19 (D64 in human Arpp19) and a lysine (K88) in the human B55 subunit. In addition, in the worm complex, we observed the nearby and conserved phenylalanine F65 (F60 in human Arpp19) stacked in between the subunits B55 and C. This residue seems to make hydrophobic contact with a leucine L126 of B55 (L87 in human B55). Other contacts are not systematically predicted in the three complexes but they may enhance the overall interaction between Arpp19 and the

PP2A phosphatase. Noteworthy, the three conserved residues surrounding the phosphorylated serine, F60, D61 and D64 in human Arpp19, seems important for precise positioning of the serine into the catalytic site of PP2A. This nicely explained the impact of their mutation to alanine, that produce variants that are rapidly dephosphorylated by PP2A-B55 and that lose their affinity for the phosphatase (Labbé *et al*, 2021).

Interestingly, no complexes could be predicted for the full-length FAM122A inhibitor with PP2A-B55 using Alphafold 2.2. On the contrary, short segments of FAM122A (from the three species used above) led to prediction of interactions between FAM122A and PP2A-B55. The interface partially overlaps with that observed for PP2A-B55-Arpp19 complexes supporting the fact that the two inhibitors compete for PP2A-B55 binding. Nevertheless, the precise interactions differ significantly. First, FAM122A does not seem to point into the catalytic site as Arpp19 seems to do, although there are also two predicted salt bridges between two glutamate residues from FAM122A (E100 and E104 in human FAM122A) with the same arginines contacting D61 and S62 of Arpp19 of the catalytic subunit of PP2A (R89 and R214 in human PP2A) (Figure 6b). These two interactions are crucial since, as shown above (Figure 3f), the corresponding E90A and E94A *Xenopus* FAM122A mutants are unable to bind the phosphatase. Finally, as expected, the second helix of FAM122A containing the putative conserved SLiM motif, interacts with the B55 subunit and this interaction takes place in a region of B55 close to the one binding α2 helix of Arpp19.

In conclusion, our modeling data obtained for Arpp19 and FAM122A interaction with PP2A-B55 using Alphafold multimer suggest that the two inhibitors would produce analogous but distinct complexes with their common target. The size of these interfaces suggests that Arpp19 would be a stronger inhibitor than FAM122A and could thus promote the dissociation of the latter. This assumption is supported by newly predicted contacts with PP2A-B55 likely playing a major role in the strong inhibition of this enzyme by Arpp19 and that include the phosphorylation of the central serine that would tightly interact with the catalytic manganese ions.

FAM122A is required *"in vivo"* for mitotic entry in the *C. elegans* germline

Our data above using ectopic FAM122A demonstrates that the addition of this protein to interphase *Xenopus* egg extracts promote mitotic entry. We thus sought to assess the impact of the depletion of the endogenous FAM122A from these extracts in mitotic entry. However, unfortunately, probably because we lost FAM122A during cytoplasmic extract purification,

we were unable to immunoprecipitate endogenous FAM122A. We thus used the nematode *Caenorhabditis elegans* as a model to investigate the role of FAM122A in PP2A-B55 inhibition and mitotic entry. The gene *F46H5.2* in *C. elegans* has been previously suggested as the putative orthologue of FAM122A protein(Kim *et al*, 2018). To confirm that it does indeed correspond to *C elegans* FAM-122A (Ce FAM-122A), we produced and purified this protein and we checked whether it was able to inhibit PP2A-B55 and to promote mitotic entry in interphase extracts. As shown in Figure 7a, dephosphorylation of S113 of Arpp19 and of T481 of PRC1 by PP2A-B55 was strongly delayed by the addition of this protein. Moreover, when supplemented to interphase extracts, Ce FAM-122A induced mitotic entry and exit (Figure 7b). Thus, the product of the gene *F46H5.2* does correspond to the FAM122A orthologue.

We then investigated the capacity of endogenous Ce FAM-122A to inhibit PP2A-B55 "*in vivo"* in the worm. To this, we first took advantage of a multivulva phenotype induced by the mutant *let-60(n1046gf)*. This mutant, corresponding to a gain of function of the human orthologue Ras, promotes the formation of several vulvas in the worm (Figure 7c). It has been shown that the multivulva phenotype induced by *let-60(n1046gf)*(Sieburth *et al*, 1999) can be attenuated by negatively modulating PP2A-B55 activity as this protein promotes Ras signalling during vulva development. Accordingly, we observed a suppression of the multivulva phenotype after depletion of SUR-6 (SUpressor of Ras-6, the orthologue of human B55 subunit of PP2A) by RNAi. In order to assess whether endogenous Ce FAM-122A acts as an inhibitor of PP2A-B55, we examined the effect of the depletion of this protein by RNAi on the multivulva phenotype induced by the *let-60(n1046gf)* mutant. If this protein is a PP2A-B55 inhibitor *"in vivo"*, its depletion should promote the reactivation of this phosphatase and thus significantly increase the presence of multivulvas in the worms. Confirming this hypothesis, the depletion of Ce FAM-122A by RNAi dramatically increased this phenotype (Figure 7c). Thus, Ce FAM-122A does act as an inhibitor of PP2A-B55 "*in vivo"*.

We further explored the role of this protein in *C. elegans* in mitosis "*in vivo"*, in *F46H5.2*^{FAM122A}*(RNAi)* treated worms. Interestingly these worms exhibit a decreased fecundity (Figure 7d) with a significant increased percentage of embryonic lethality at 25°C (median: 8.4% in RNAi-treated vs 0.30% in controls; $p<0.0001$) and a double number of unfertilized eggs than controls (median 26.18 % in RNAi-treated vs 12.10% in controls; $p<0.014$) (Figure 7e). Even wildtype *C. elegans* can produce unfertilized eggs when they age however, *F46H5.2*^{FAM122A}(RNAi) worms display this phenotype on their first day of adulthood. These results suggest a fertility defect and led us to explore the function of the

reproductive system. We thus investigated cell division within the *C. elegans* germline using nematode strains expressing histone and gamma-tubulin tagged with GFP under a germline and embryonic promoter. We focused on mitotic division of the germline stem cells of the distal gonad. Using chromatin and centrosome as proxy of mitotic progression(Gerhold *et al*, 2015), we counted the number of stem cells in interphase and in mitosis (Appendix Figure S6). We observed a significant reduction of interphase cells and an increase in mitotic cells in RNAi treated worms (Figure 8a). Interestingly, the number of cells in prophase (assessed by the presence of two separating centrosomes and a circular intact nuclei), was also dramatically increased, although some cells could progress into mitosis, probably due to a partial depletion of FAM-122A. However, these cells displayed a perturbed mitotic progression since we observed a drop of the number of anaphases (Figure 8b). These data suggest that depletion of *F46H5.2* gene product decreases the capacity of germline stem cells to enter into mitosis and perturbs their progression through this phase of the cell cycle. To further investigate this hypothesis, we used a cell line with GFP-tagged gamma-tubulin and with RFP-tagged histone in which we followed by time lapse microscopy the duration of mitosis. We considered mitosis duration as the time from first centrosome separation movement starts to anaphase onset. As depicted in Figure 8c, stem cells from control worms displayed a rapid mitosis, with a timing around 21 minutes. Conversely, most Ce FAM-122A depleted stem cells, stayed with separated centrosome throughout the time of the experiment (40 to 50 minutes) indicating that these cells were arrested or highly delayed in prophase. We observed fewer cells entering mitosis in the FAM-122A depleted worms (Figure 8c, upper graph). In addition, although they did not display differences in the timing from nuclear envelope breakdown to metaphase (congression), they showed a significant increase of the time required for anaphase onset (Figure 8c, lower graph). This delay is in accord with the drop of the number of anaphase in RNAi-treated germline stem cells and suggests that FAM122A-dependent inhibition of PP2A-B55 could not be only required for mitotic entry, but could also be essential again during mitotic exit to promote anaphase onset when Gwl and cyclin B/Cdk1 become inactivated by cyclin B proteolysis.

Endogenous FAM122A proteins accumulates during G2 in human cells

How cyclin B/Cdk1 is triggered at G2-M is a main question yet to be answered. To activate cyclin B/Cdk1, Wee1/Myt1 and Cdc25 have to be phosphorylated. To that, an increase of the activity of cyclin A/Cdk, as well as a drop of PP2A-B55 are essential. The fact that FAM122A does not require phosphorylation to inhibit PP2A-B55 at the endogenous

concentration and that cyclin A/Cdk is a poor substrate of Myt1 kinase during G2 (Coulonval *et al*, 2003; Booher *et al*, 1997) make of these two factors good candidates for triggering mitosis. However, to promote G2-M transition, it is essential that these two proteins accumulate during G2 to reach sufficient levels to revert cyclin B/Cdk1 inhibition. Accumulation of cyclin A has been largely demonstrated in the bibliography. Much less is known about the levels of FAM122A during G2. We thus measured the levels of FAM122A throughout the cell cycle in RPE1 cells. Interestingly, as depicted in Figure 8d, FAM122A protein accumulates during G2 reaching maximal level at G2-M transition concomitantly with cyclin A accumulation. Moreover, the amount of these two proteins rapidly decrease during mitotic progression supporting the hypothesis of a putative role of these two proteins in triggering cyclin B/Cdk1 activation and mitotic entry

DISCUSSION

Protein phosphorylation plays a major role in the control of cell cycle progression. This phosphorylation results from a fine-tuned balance between the activities of cyclin/Cdk complexes and phosphatases. The modulation of the phosphatase PP2A-B55 is key for S and M phases. During DNA replication, PP2A-B55 has to be inhibited to maintain the phosphorylation of the replication factor Treslin responsible of origin firing, while at G2-M, the negative modulation of this phosphatase is essential for cyclin B/Cdk1 activation.

To enter into mitosis, a partial pool of cyclin B/Cdk1 has to be turned on to induce the amplification loop that triggers cyclin B/Cdk1 full activation via Wee1/Myt1/Cdc25 phosphorylation. However, Wee1/Myt1/Cdc25 phosphorylation can be also achieved if PP2A-B55 is at least partially inhibited. This inhibition depends on the phosphorylation of Arpp19/ENSA and thus, requires the activity of its upstream kinase Gwl. However, at M entry, both Gwl and cyclin B/Cdk1 are inactive and their activation depends on each other. Thus, none of them can be the initial event triggering mitosis.

In this study we investigated the role of FAM122A, a new identified regulator of PP2A-B55, in triggering mitotic entry. Using *Xenopus* egg extracts we demonstrate that the negative regulation of PP2A-B55 by FAM122A does not induce Wee1 or PP2A catalytic subunit proteolysis as previously proposed (Fan *et al*, 2016; Li *et al*, 2020). Conversely, it promotes mitotic entry by directly binding and inhibiting the activity of this phosphatase. PP2A-B55 inhibition by FAM122A precedes Gwl and cyclin B/Cdk1 activation since its phosphorylation is not required to negatively modulate the phosphatase, although we cannot exclude an additional positive modulation of its activity by this posttranslational modification.

However, FAM122A-dependent induction of mitosis depends on cyclin A/Cdk, indicating that FAM122A promotes M-Phase entry by promoting cyclin A/Cdk-dependent phosphorylation. We, thus, hypothesize that the initial event triggering mitotic entry corresponds to the accumulation of FAM122A and cyclin A/Cdk1 that would result in a first burst of FAM122A-dependent inhibition of PP2A-B55 and the subsequent cyclin A/Cdk1-dependent phosphorylation of Cdc25 and Myt1. This will in turn result in the full activation of cyclin B/Cdk1 and mitotic entry (Figure 9). Accordingly, our data show that, as for cyclin A/Cdk, FAM122A protein accumulates during G2, reaching a maximum level at G2-M transition. We additionally show that FAM122A plays a key role in PP2A-B55 inhibition and mitotic entry "*in vivo*" in the *C. elegans* model in which, FAM122A knockdown modulates phosphatase activity during vulval development and prevents mitotic entry in germ line stem cells.

Remarkably, a very low dose of FAM122A (15 nM) is sufficient to promote mitotic entry when added to interphase extracts. This dose would correspond to about 15% of the total concentration of PP2A-B55 present in these extracts (100-300 nM (Mochida *et al*, 2009)) suggesting that, the inhibition of a very small proportion of this phosphatase, would be enough to reverse the balance towards mitotic substrate phosphorylation. Alternatively, FAM122A localization could also play an essential role by locally inhibiting the phosphatase at the vicinity of cyclin A/Cdk kinase permitting the phosphorylation of its substrates.

However, strikingly, although FAM122A clearly binds PP2A-B55 during interphase, we discovered that this protein rapidly dissociates from the phosphatase as soon as the extract entered into mitosis and re-associates again upon mitotic exit. Our data show that this dissociation is induced by the phosphorylation of Arpp19 by Gwl. Accordingly, the addition of phospho-S71-Arpp19 to interphase extracts or to FAM122A-PP2A-B55 pull-downs promotes the exchange of FAM122A by phospho-S71-Arpp19 in the PP2A-B55 complex. These data indicate that, when phosphorylated by Gwl, Arpp19 competes with FAM122A and promotes its dissociation from the phosphatase. Indeed, our data demonstrate that phospho-S71-Arpp19 has a 100-fold lower K_i than FAM122A indicating that p-S71-Arpp19 displays much higher affinity, inhibitory activity and binding to PP2A-B55 than FAM112A. Accordingly, in our analysis, endogenous phospho-S71-Arpp19 is able to dissociate ectopic His-FAM122A from PP2A-B55 even when the latter is present in the extract at a molar concentration 215 times higher than the former. These properties were supported by the structure predictions of FAM122A- and Arpp19-PP2A-B55 complexes obtained by AlphaFold2.2. Interestingly, structures predicted for FAM122-PP2A-B55 and

phospho-Arpp19-PP2A-B55 complexes superposed from three different species (human, *Xenopus* and *C. elegans*) revealed that FAM122A and phospho-S71-Arpp19 inhibit the phosphatase by competing with the substrate through directly blocking its access, a hypothesis that is also supported by our kinetics experiments that confirm the competitive model as the best fitting our data. However, FAM122A and phospho-S71-Arpp19 display different interactions with the PP2A-B55 heterocomplex. FAM122A weakly interacts with the C subunit via two glutamic acids forming salt bridges with two arginine residues of the C subunit of PP2A. These interactions locate the second alpha helix of this protein on the surface of the catalytic site occluding, in this way, substrate entry. Conversely, phospho-S71-Arpp19 tightly binds PP2A C mostly because of the presence of the phospho-serine residue that would directly interact with manganese ions of the catalytic site, an interaction that would be stabilized by two supplementary salt bridges formed with two arginine of the C subunit. This tight interaction can be only dissociated upon Arpp19 dephosphorylation, however, as previously reported, dephosphorylation of the Arpp19 Gwl-site is very slow compared to regular substrates of this phosphatase making of this phosphoprotein a potent inhibitor of PP2A-B55 (Labbé *et al*, 2021; Williams *et al*, 2014). These data nicely explain the different affinities for P22A-B55 of FAM122A and p-S71-Arpp19, however, it is worth highlighting that, the 2 Mn^{2+} divalent cations present in the bacterial purified PP2A-B55 complex used for structural studies, do not reflect the native PP2A-B55 enzyme that contains a Zn2+: Fe2+ ion pair (Brautigan & Shenolikar, 2018), a feature that could modify the interaction of p-S71-Arpp19 to the phosphatase. However, during the review process of this manuscript, new cryo-EM structures of the complex of FAM122A or Arpp19 with purified PP2A-B55 from human cells were published (Padi *et al*, 2024). Interestingly, these structural results confirm our modelling predictions and kinetic data and reinforce the idea that FAM122A and Arpp19 interphases with PP2A-B55 partially overlap. Moreover, according with our model, data also support a role of the phosphorylation of Arpp19 central serine in tightly interacting with the native ions of the catalytic site of the C subunit providing a stronger phosphatase inhibitory activity to this protein compared to FAM122A. However, besides cryo-EM results, authors also presented NMR data suggesting a simultaneously binding of a C-terminal truncated FAM122A and Arpp19 with a loopless B55 form, a B55 variant unable to bind PP2A A subunit. However, whether this trimer can be also observed with the wildtype Arpp19 and FAM122A and the functional PP2A-B55 heterocomplex is not clear. Indeed, these would be very surprising since, as supported by the authors themselves, these two inhibitors interact with the same or very close residues of B55 and C subunits of the phosphatase making highly

unlikely the presence of a Arpp19/FAM122A/PP2A-B55 trimer. In this line, our data clearly stablish a dissociation of FAM122A from PP2A-B55 when both proteins are incubated with the phosphatase both in *in vitro* pulldown experiments and *in extracto*.

Importantly, our data additionally show that FAM122A is dissociated from PP2A-B55 by phospho-Arpp19 (S71) during mitosis. Although we do not know what could be the role of this dissociation, we predict that it could be physiological relevant and required to induce a correct mitotic progression. In this line, it is possible that a higher PP2A-B55 inhibitory activity is required during mitotic progression to permit the late mitotic substrate phosphorylation. In agreement with this hypothesis, previous data demonstrate that cyclin B1/Cdk1 levels required to enter mitosis are lower than the amount of cyclin B1–Cdk1 needed for mitotic progression (Lindqvist *et al*, 2007). Moreover, besides the high inhibitory activity of phospho-S71-Arpp19, the fact that its dissociation from PP2A-B55 is gradually induced by dephosphorylation could be also essential to establish the temporal pattern of mitotic substrate dephosphorylation required for the correct order of mitotic events during mitotic exit.

In summary, we identified a new role of FAM122A in promoting G2-M transition through the inhibition of PP2A-B55 and we provided data indicating that cyclin A/Cdk, together with FAM122A-dependent inhibition of PP2A-B55 promote Gwl and cyclin B/Cdk1 activation and trigger mitotic entry. Finally, we showed that, upon mitotic entry, FAM122A is dissociated from PP2A-B55 by phospho-Arpp19 until the time when Gwl inactivation and Arpp19 becomes fully dephosphorylated permitting to FAM122A to re-associate again to the phosphatase.

MATERIALS & METHODS

"In vitro" phosphorylation

Phosphorylation of Arpp19 on S71 or of *Xenopus* FAM122A by Gwl was induced by using GST-K72M hyperactive mutant form of Gwl purified from SF9 cells. For *"in vitro"* phosphorylation reaction, *Xenopus* His-Arpp19 protein or His-FAM122A and GST-K72M Gwl kinase were mixed at a final concentration of 133 and 67 µM for the two first proteins and 0.34 µM for the last one in a reaction buffer containing $7x10^{-2}$ µM ATPγ^{33}P at a specific activity of 3000 Ci/ mmol, 200 µM ATP, 2 mM $MgCl_2$ and Hepes 50 mM, pH 7,5.

For phosphorylation of Arpp19 on S113 by PKA, a final concentration of 33 µM of Arpp19 and 1.25 µM of His-PKA catalytic subunit purified from His-tag column were mixed to the

reaction buffer containing $8x10^{-3}$ µM ATPγ^{33}P at a specific activity of 3000 Ci/ mmol, 200 µM ATP, 2 mM $MgCl_2$, 100 mM NaCl and 50 mM Tris pH 7.5.

For phosphorylation of GST-PRC1 on T481, Cdk1 activity was obtained by immunoprecipitation. In brief, His-human cyclin A was mixed with CSF extracts at a final concentration of 0.2 µM for 30 minutes and subsequently supplemented with 50 µl of protein G magnetic Dynabeads pre-linked with 10 µg of *Xenopus* Cdk1 C-terminus antibodies. After 45 minute-incubation the beads were washed 3 times with 500 mM NaCl, 50 mM Tris pH 7.5, twice with 100 mM NaCl, 50 mM Tris pH 7.5 and finally resuspended with 100 µl of reaction buffer containing 1mM ATP, 2 mM $MgCl_2$, 100 mM NaCl and 50 mM Tris pH 7.5. GST-PRC1 was then added to the beads at a final concentration of 21 µM.

For thio-phosphorylation of Arpp19 on S71, His-tag of His-Arpp19 protein was removed using TEV protease. Non-tagged Arpp19 was then used for phosphorylation at a final concentration of 66 µM in presence of 1mM ATPγS, 2 mM $MgCl_2$, 100 mM NaCl, 50 mM Tris pH 7.5 and 0.34 µM of GST-K72M Gwl kinase.

All *"in vitro"* phosphorylation reactions were incubated for 1 h, aliquoted and frozen at -70°C until use.

Dephosphorylation reactions in kinase inactivated extracts

When the impact of *Xenopus*, human, or *C. elegans* FAM122A proteins on either S113 Arpp19 or T481 PRC1 dephosphorylation was checked in ATP-devoid interphase extracts, 1 µl of the corresponding *"in vitro"* phosphorylation reaction was mixed to 1 µl His-FAM122A to a final concentration of 14.3 µM, diluted with 8 µl of Tris 50 mM-10 mM EDTA buffer and supplemented with 10 µl of ATP-devoid interphase extracts adjusted to 500 mM NaCl with a solution of 5M NaCl and a sample of 2 µl was recovered at the indicated time-points.

Immunoprecipitation/Immunodepletion

Immunodepletions were performed using 20 µl of extracts, 20 µl of G-magnetic Dynabeads (Life Technologies), and 2 µg of each antibody except for cyclin A for which we used 3.3 µl. Antibody-linked beads were washed 2 times with XB buffer, 2 times with Tris 50 mM, pH 7.5 and incubated for 15 min at room temperature (RT) with 20 µl of *Xenopus* egg extracts. The supernatant was recovered and used for subsequent experiments. To fully deplete endogenous proteins, two rounds of immunodepletion were performed.

For Gwl rescue experiments, a final concentration of 19.2 nM of K72M GWL was added to depleted egg extracts and a sample of 2 µl was recovered and used for western blot.

For histidine pulldown experiments, 20 µl of interphase or CSF extracts containing His-*Xenopus* or His-human FAM122A proteins, were supplemented with 20 µl of HisPur^{TM}NiNTA Magnetic beads (Life Technologies) at a final concentration of 7.15 µM and incubated for 10 minutes of continuous mixing at 21°C. Upon centrifugation, beads are washed twice with XB buffer and supplemented with Laemmli sample buffer for western blot use.

Protein purification

His-*Xenopus* Arpp19, His-*Xenopus* wildtype and mutant of FAM122A in which all serine and threonine residues were mutated into alanine, as well as, His-human FAM122A, His-*C elegans* FAM122A, His-human PRC1, and His-Rat Catalytic Subunit of PKA were produced in *Escherichia coli* and purified using TALON Superflow Metal Affinity Resin. GST-*Xenopus* FAM122A protein was produced in *Escherichia coli* and purified using a glutathione column.

CSF, interphase and kinase-inactivated egg extracts

Frogs were obtained from « TEFOR Paris-Saclay, CNRS UMS2010 / INRAE UMS1451, Université Paris-Saclay», France and kept in a *Xenopus* research facility at the CRBM (Facility Centre approved by the French Government. Approval n° C3417239). Females were injected of 500 U Chorulon (Human Chorionic Gonadotrophin) and 18 h later laid oocytes were used for experiments. Adult females were exclusively used to obtain eggs. All procedures were approved by the Direction Generale de la Recherche et Innovation, Ministère de L'Enseignement Supérieur de la l'Innovation of France (Approval n° APAFIS#40182-202301031124273v4).

Metaphase II-arrested egg extracts (CSF extracts) were obtained by crushing metaphase II-arrested oocytes in the presence of EGTA at a final concentration of 5 mM(Lorca *et al,* 2010).

Interphase *Xenopus* egg extracts were obtained from metaphase II-arrested oocytes 35 minutes after Ca^{2+} Ionophore (final concentration 2 µg/ml) treatment.

To measure the capacity of FAM122A to promote mitotic entry, 20 µl of CSF or Interphase extracts were supplemented with a final concentration of 7.15 µM of *Xenopus*, human or *C elegans* FAM122A proteins.

For dephosphorylation assays kinase inactivated interphase extracts were mixed with Arpp19 or PRC1 proteins *"in vitro"* phosphorylated by PKA or by cyclin A/Cdk1 respectively at a final concentration of 1.65 µM together with *Xenopus* or human FAM122A at a final concentration of 14.3 µM.

Kinase-inactivated egg extracts were obtained from dejellied unfertilised eggs transferred into MMR solution (25 mM NaCl, 0.5 mM KCl, 0.25 $MgCl_2$, 0.025 mM NaEGTA, 1.25 mM HEPES-NaOH pH7.7), washed twice with XB Buffer (50 mM sucrose, 0.1 mM $CaCl_2$, 1 mM $MgCl_2$, 100 mM KCl, HEPES pH 7.8) and centrifuged twice for 20 minutes at 10 000 g. Cytoplasmic fractions were then recovered, supplemented with RNAse (10 µg/ml final concentration) and dialyzed versus a solution of 50 mM Tris pH 7.7, 100 mM NaCl overnight to eliminate ATP. Upon dialysis, extracts were ultracentrifuged for 50' at 300 000 g and supernatant recovered for use.

Calculation the K_i values for FAM122A and p-S71-Arpp19 inhibitors

Arpp19 phosphorylated on S113 by PKA was mixed with kinase inactivated interphase extracts at final concentrations of 120, 180, 300, 600, 1200 and 2000 nM. Since at lower concentrations of p-S113-Arpp19, the substrate is more rapidly dephosphorylated, a dilution of the PP2A-B55 phosphatase was required to record sufficient dephosphorylation experimental points on these initial linear phases. We thus diluted the extracts from 1/50 to 1/200 when the concentration of p-S113-Arpp19 varied from 120 to 2000 nM. Upon substrate addition to the extracts, an aliquot was taken every one or two minutes until 7 or 14 minutes respectively, depending on the substrate concentration. The reaction was stopped by adding Laemmli blue buffer and heating for 5 minutes at 90°C.

Dephosphorylation was measured by western blot using anti-pS113-Arpp19 antibody, a secondary goat anti-rabbit DyLight 800 conjugated antibody and quantified by Li-cor Odysey M System. Inhibition constants (K_i) were determined by repeating these experiments at different concentrations of FAM122A (50, 125 and 250 nM) or Thio-S71-Arpp19 (1, 2 and 3 nM). Values of the steady state rate constants, k_{ss}, were determined using GraFit 7.0.3 software (Erithacus software) from the slope of the initial linear phases of the reaction time courses. The actual sampling times were normalized by dividing by the enzyme dilution factor, so that all experiments could be combined for global fitting procedures. Global fittings were performed on the raw data with GraFit 7.0.3 software using four different inhibition modes: competitive, non-competitive, mixed and uncompetitive. Times courses and

secondary curves and the corresponding Lineweaver-Burk representations are shown as Appendix Materials (Appendix Figures S3 and S4).

Plasmids

Xenopus wildtype and the Δ(1-73) and serine/threonine-to-alanine mutant form (accession number NP_001085566.1) cDNAs, as well as human (accession number NP_612206.5), and *C elegans* (accession number NP_001024675.1) cDNAs were synthesized by GeneCust (France) and subcloned into the HindIII-XhoI site of pET14b for human FAM122A, into the NdeI-BamHI site of pET14b for *C elegans*, into the XhoI-BamHI site of pET14b for *Xenopus* wildtype and mutant forms and into the BamHI-XhoI site of pGEX4T1 for wildtype *Xenopus* FAM122A.

Antibodies

Xenopus, human and *C elegans* FAM122A protein was detected using anti-histidine antibodies. Antibodies used in this study are detailed in Appendix Table S1.

Mutagenesis

Deletions and single-point mutations of *Xenopus* FAM122A were performed using Pfu ultra II fusion DNA polymerase. Oligonucleotides were purchased from Eurogentec and are detailed in the Appendix Table S2.

***C. elegans* culture and RNAi mediated depletion.**

C. elegans worm strains N2 (wildtype ancestral, Bristol) and MT2124 (*let-60(gf)*) were obtained from the CGC (https://cgc.umn.edu) and maintained at 20 °C on NGM plate using standard procedures(Brenner, 1974) except that worms were fed with HT115 bacteria to standardize their growth condition with the RNAi mediated depletion. RNAi feeding was performed as described previously (Kamath *et al*, 2001). HT115 thermocompetent *E. coli* were transformed with L4440 empty vector (control) or containing a sequence targeting, SUR-6^{PP2AB} or F46H5.$2^{FAM122A}$. The L4440 vector targeting F46H5.$2^{FAM122A}$ was generated using a fragment amplified from *C. elegans* cDNA corresponding to 715 bp of the coding sequence (nucleotides 398 to 1112) which was subsequently inserted between XhoI and NotI restriction enzyme sites in L4440 vector. Control, SUR-6^{PP2AB} vector come from the Arhinger's library. In a 14 ml culture tubes, 2 ml of LB medium supplemented with 100 µg/mL of ampicillin were inoculated with a colony of HT115 bacteria transformed with

respective L4440 vectors and incubated at 37 °C under agitation. After 7 h, 200 µl of this bacterial culture was transferred on a 60 mm diameter NGM plate containing 0.2 mM IPTG and 50 µg/ml of carbenicillin. Plates were allowed to dry overnight at room temperature, stored at 4 °C and used within 48 h. Worms were synchronized using the alkaline bleach method (1.2% NaOCl, 250 mM KOH in water (Stiernagle, 2006)). Eggs obtained from the alkaline bleach were allowed to hatch overnight at 16 °C in M9 buffer. To score FAM122A effect on Ras (*let-60(gf))* induced multivulva phenotype, around 200 synchronized larvae were placed on a single feeding plate and incubated 66-72 h at 20 °C until control worms reach adulthood. Phenotypes were scored at the time where the first eggs laid by control worms started to hatch to ensure that all worms fully develop to the adult stage. Vulval defect phenotypes was scored under a dissecting scope by counting the total number of worms and the number of worms exhibiting multiple vulva. The counting was repeated once for each plate to minimize scoring errors. Representative images of vulval phenotypes were acquired with a scMOS ZYLA 4.2 M camera on a Zeiss Axioimager Z2 and a 20X Plan Apochromat 0.8 NA using worms immobilized with a solution of 10 mM sodium azide and mounted on an 3 % agarose pad in between a microscopy slide and a cover glass.

Live imaging of *C. elegans*

For "*in vivo"* imaging, we used nematode strains expressing GFP-gamma-tubulin and GFP-histone (TH32: unc-119(ed3), ruIs32[pAZ132; pie-1/GFP::histone H2B] III; ddIs6[GFP::tbg-1; unc-119(+)] V or GFP-tubulin and histone-mCherry (JDU19: *ijmSi7 [pJD348; Pmex-5_gfp::tbb-2; mCherry::his-11; cb-unc-119(+)] I; unc-119(ed3) III)* and JDU233: *ijmSi63 [pJD520; mosII_5'mex-5_GFP::tba-2; mCherry::his-11; cb-unc-119(+)] II; unc-119(ed3) III*) kindly provided by Julien Dumont (Institut Jacques Monod, Paris). Worms were cultured at 25 °C and bacterial feeding was performed similarly to the multivulva experiment, except that worms were not synchronized by alkaline bleach. Instead, 6 worms were allowed to lay eggs on a 60 mm diameter NGM feeding plate. After 2 h at 25 °C adults were removed and their progeny was allowed to develop on the feeding plate and at 25 °C for 44-52 h until the first adults start to lay eggs (young adults). Worms were anesthetized in 0.02 % tetramisole in M9 buffer for 10 min before being transferred onto a 4 % agarose pad (Laband *et al*, 2018) . The pad was then covered with 22x22 mm coverslip and sealed with VaLaP (vaseline and paraffin wax and lanolin, 1:1:1). The chamber was filled with M9 to prevent drying and to dilute tetramisole. Immobilized worms were imaged for a maximal time of 50 min and were not maintained more than one hour after being removed from their feeding plate. Germline

stem cell division imaging was performed according to Gerhold et al.(Gerhold *et al*, 2015). To minimize toxicity, we used minimal laser intensity and exposure using a spinning disk confocal Yokogawa W1 on an Olympus inverted microscope coupled to a sCMOS Fusion BT Hamamatsu camera. Long-term live imaging (up to 50 min) was performed with a 30x UPLSAPO 1.05 NA DT 0.73 mm silicone objective by taking a full z-stack of the entire worms (~40 µm) with 2 µm steps every 20 s or 30 s. For higher resolution images and to score mitotic phases using centrosome and chromatin markers, a single z-stack was performed on each worm with a 1 µm z-section and using a 60x UPLSAPO 1.3 NA DT 0.3 mm silicone objective.

Analysis of germline stem cells divisions.

Images and movies were visualized using ImageJ or CellSens visualization software (OlyVIA, Olympus). Analysis of germline stem cells divisions was made following a previous article from Gerhold et al. (Gerhold *et al*, 2015). Accordingly, timing of prophase corresponds to the initiation of centrosome separation (GFP-tubulin) to the beginning of chromosome congression monitored using the mCherry-histone. As ovulation generates movement within the gonad arm, cells can move in 3D, therefore tracking of individual cell progression was performed by navigating throughout z-stack over time. Representative images and montages in the Figure 8 correspond to a maximal intensity projection of 4-5 z-sections (8-10 µm). To quantify the number of cells in each respective cell cycle phases, we used GFP-histone and GFP-gamma-tubulin signal to monitor centrosome separation, nuclear envelope breakdown, chromosome congression and separation. The number of stem cells in the mitotic zone of the distal gonad was estimated by counting the number of nuclei based on histone signal. Here, cells were considered in prophase when having 2 separating or opposed centrosomes (spots) closed to nuclei or condensed chromosomes. Metaphase and anaphase correspond respectively to a single plate or two separated plates of tightly condensed chromosomes.

Protein structure modelling

Complexes of PP2A-B55 with Arpp19/ENSA or FAM122A were produced using Alphafold_Multimer version 2.2 (preprint: Evans *et al*, 2021) with the protein sequences from three species (*C. elegans*, *X. laevis* and *H. sapiens*). Manganese ions were added to the resulting models by superposition and extraction from the crystal structure of PP2A (PDB3DW8). The phosphoserine was modelled by superposing a phosphoserine onto the

corresponding serine in each complex of interest and searching for the best orientation using our recent webserver ISPTM2 (https://isptm2.cbs.cnrs.fr). Because full-length FAM122A sequences led to no interactions as predicted by Alphafold 2.2, truncated version of FAM122A were used instead. For the human, *Xenopus*, and worm sequences, the shortened versions comprised residues 84 to 117, 61 to 120 and 70 to 149, respectively.

Cell culture and synchronization.

RPE1 cells were maintained adherent using standard cell culture procedures in DMEM-F12 medium supplemented with 10 mM HEPES pH 7.2, 10% of fetal bovine serum and antibiotics (penicillin, streptomycin). Synchronization of cells at the G1/S boundary was achieved by a double thymidine block. In brief, cells were plated at 14,000 cells per cm^2 in 6 cm diameter petri dishes and, 24 h later, incubated for 18 h in medium containing 2 mM thymidine. Cells were then washed twice with 1xPBS to remove excess of thymidine and fresh medium containing 25 µM of 2'-deoxycytidine was added for 8-9 h. Cells were washed twice with 1xPBS and a second block was performed by adding medium containing 2 mM of thymidine for 18h. Release of G1/S arrested cells was performed by washing twice with 1xPBS and exchanging the medium for fresh medium containing 25 µM of 2'-deoxycytidine. Cells were collected at 0, 4, 6, 7, 8 and 9 h after release. Cells were collected and analysed by western blot analysis and flow cytometry (FACS). For western blot analysis, 40 µg of total protein were loaded and separated by SDS-PAGE using 10% acrylamide gels. Proteins were then transferred onto a PVDF membrane compatible with fluorescent analysis. Protein amounts were measured by western blot using polyclonal anti-FAM122A (1/1000) and anti-cyclin A (1/2000) and monoclonal anti-βTubulin (1/2000) primary antibodies and with goat anti-rabbit Dylight 680 conjugated and goat anti-mouse Dylight 800 conjugated fluorescent secondary antibodies and quantified by Li-cor Odysey M System. For cell sorting analysis, after ice-cold 70% ethanol fixation at -20°C, cells were resuspended and incubated for 5 min in 500 µL of 0.4%TritonTX100, 3% BSA in 1xPBS for cell permeabilization. DNA staining was then performed by adding 300 µL of 1xPBS containing 3% BSA, 0,01 µg/mL of 7-AAD and 0.01 mg/mL RNAse A. Cells were incubated in the dark for one hour at room temperature, washed 2 times with 1xPBS supplemented with 3% BSA by centrifugation (3 min at 400xg) and resuspend in 130 µL prior to cell sorting using Novocyte flow cytometer system.

Data Availability

Live imaging data sets used in this manuscript are available on BioImage Archive with the accession number: S-BIAD984. https://www.ebi.ac.uk/biostudies/bioimages/studies/S-BIAD984.

ACKNOWLEDGMENTS

We are grateful to Marc Plays and Phillipe Richard for animal and antibody production and to MRI for microscopy facility. We thank Julien Dumont (Institut Jacques Monod, Paris) for kindly providing GFP-gamma-tubulin and GFP-histone nematode strains and Lucie Van Hove, Sylvain Roque, Morgane Robert, Lucie Van Hove (LP lab) and Celia Benchoug for their technical help. This work was supported by the Agence National de la Recherche (REPLIGREAT, ANR-18-CE13-0018-01, MITODISSECT, ANR-22-0022 and MTDiSco, ANR-20-CE13-0033), La Ligue Nationale Contre le Cancer (Equipe Labellisée, EL2019 CASTRO and EL2018 PINTARD), Ligue Nationale Contre le Cancer (Comité Département 66/ LACROIX), the French Infrastructure for Integrated Structural Biology (FRISBI, ANR-10-INSB-005 and the infrastructure ChemBioFrance. Some nematode strains were provided by the CGC, which is funded by NIH Office of Research Infrastructure Programs (P40 OD010440).

Disclosure and competing interests statement

The authors declare no competing interests.

REFERENCES

Alvarez-Fernandez M, Sanchez-Martinez R, Sanz-Castillo B, Gan PP, Sanz-Flores M, Trakala M, Ruiz-Torres M, Lorca T, Castro A & Malumbres M (2013) Greatwall is essential to prevent mitotic collapse after nuclear envelope breakdown in mammals. *Proceedings of the National Academy of Sciences of the United States of America* 110: 17374–9

Blake-Hodek KA, Williams BC, Zhao Y, Castilho PV, Chen W, Mao Y, Yamamoto TM & Goldberg ML (2012) Determinants for activation of the atypical AGC kinase Greatwall during M phase entry. *Molecular and cellular biology* 32: 1337–53

Booher RN, Holman PS & Fattaey A (1997) Human Myt1 Is a Cell Cycle-regulated Kinase That Inhibits Cdc2 but Not Cdk2 Activity*. *Journal of Biological Chemistry* 272: 22300–22306

Brautigan DL & Shenolikar S (2018) Protein Serine/Threonine Phosphatases: Keys to

Unlocking Regulators and Substrates. *Annual Review of Biochemistry* 87: 921–964

Brenner S (1974) The genetics of Caenorhabditis elegans. *Genetics* 77: 71–94

Burgess A, Vigneron S, Brioudes E, Labbe JC, Lorca T & Castro A (2010) Loss of human Greatwall results in G2 arrest and multiple mitotic defects due to deregulation of the cyclin B-Cdc2/PP2A balance. *Proceedings of the National Academy of Sciences of the United States of America* 107: 12564–9

Coulonval K, Bockstaele L, Paternot S & Roger PP (2003) Phosphorylations of cyclin-dependent kinase 2 revisited using two-dimensional gel electrophoresis. *J Biol Chem* 278: 52052–52060

Cundell MJ, Bastos RN, Zhang T, Holder J, Gruneberg U, Novak B & Barr FA (2013) The BEG (PP2A-B55/ENSA/Greatwall) Pathway Ensures Cytokinesis follows Chromosome Separation. *Molecular Cell* 52: 393–405

Evans R, O'Neill M, Pritzel A, Antropova N, Senior A, Green T, Žídek A, Bates R, Blackwell S, Yim J, *et al* (2021) Protein complex prediction with AlphaFold-Multimer. 2021.10.04.463034 doi:10.1101/2021.10.04.463034 [PREPRINT]

Fan L, Liu M-H, Guo M, Hu C-X, Yan Z-W, Chen J, Chen G-Q & Huang Y (2016) FAM122A, a new endogenous inhibitor of protein phosphatase 2A. *Oncotarget* 7: 63887–63900

Fowle H, Zhao Z, Xu Q, Wasserman JS, Wang X, Adeyemi M, Feiser F, Kurimchak AN, Atar D, McEwan BC, *et al* (2021) PP2A/B55α substrate recruitment as defined by the retinoblastoma-related protein p107. *eLife* 10: e63181

Gerhold AR, Ryan J, Vallée-Trudeau J-N, Dorn JF, Labbé J-C & Maddox PS (2015) Investigating the Regulation of Stem and Progenitor Cell Mitotic Progression by In Situ Imaging. *Current Biology* 25: 1123–1134

Gharbi-Ayachi A, Labbé J-C, Burgess A, Vigneron S, Strub J-M, Brioudes E, Van-Dorsselaer A, Castro A & Lorca T (2010) The Substrate of Greatwall Kinase, Arpp19, Controls Mitosis by Inhibiting Protein Phosphatase 2A. *Science* 330: 1673–1677

Hached K, Goguet P, Charrasse S, Vigneron S, Sacristan MP, Lorca T & Castro A (2019) ENSA and ARPP19 differentially control cell cycle progression and development. *The Journal of Cell Biology* 218: 541–558

Kamath RS, Martinez-Campos M, Zipperlen P, Fraser AG & Ahringer J (2001) Effectiveness of specific RNA-mediated interference through ingested double-stranded RNA in Caenorhabditis elegans. *Genome Biol* 2: RESEARCH0002

Kim W, Underwood RS, Greenwald I & Shaye DD (2018) OrthoList 2: A New Comparative

Genomic Analysis of Human and Caenorhabditis elegans Genes. *Genetics* 210: 445–461

Laband K, Lacroix B, Edwards F, Canman JC & Dumont J (2018) Live imaging of C. elegans oocytes and early embryos. *Methods Cell Biol* 145: 217–236

Labbé JC, Vigneron S, Méchali F, Robert P, Roque S, Genoud C, Goguet-Rubio P, Barthe P, Labesse G, Cohen-Gonsaud M, *et al* (2021) The study of the determinants controlling Arpp19 phosphatase-inhibitory activity reveals an Arpp19/PP2A-B55 feedback loop. *Nat Commun* 12: 3565

Lemonnier T, Daldello EM, Poulhe R, Le T, Miot M, Jessus C & Dupré A (2019) The M-phase regulatory phosphatase PP2A-B55δ opposes protein kinase A on Arpp19 to initiate meiotic division Cell Biology

Li F, Kozono D, Deraska P, Branigan T, Dunn C, Zheng X-F, Parmar K, Nguyen H, DeCaprio J, Shapiro GI, *et al* (2020) CHK1 Inhibitor Blocks Phosphorylation of FAM122A and Promotes Replication Stress. *Mol Cell* 80: 410-422.e6

Lindqvist A, Zon W van, Rosenthal CK & Wolthuis RMF (2007) Cyclin B1–Cdk1 Activation Continues after Centrosome Separation to Control Mitotic Progression. *PLOS Biology* 5: e123

Lorca T, Bernis C, Vigneron S, Burgess A, Brioudes E, Labbe JC & Castro A (2010) Constant regulation of both the MPF amplification loop and the Greatwall-PP2A pathway is required for metaphase II arrest and correct entry into the first embryonic cell cycle. *Journal of cell science* 123: 2281–91

Mochida S, Ikeo S, Gannon J & Hunt T (2009) Regulated activity of PP2A-B55 delta is crucial for controlling entry into and exit from mitosis in *Xenopus* egg extracts. *The EMBO journal* 28: 2777–85

Mochida S, Maslen SL, Skehel M & Hunt T (2010) Greatwall Phosphorylates an Inhibitor of Protein Phosphatase 2A That Is Essential for Mitosis. *Science* 330: 1670–1673

Padi SKR, Vos MR, Godek RJ, Fuller JR, Kruse T, Hein JB, Nilsson J, Kelker MS, Page R & Peti W (2024) Cryo-EM structures of PP2A:B55–FAM122A and PP2A:B55–ARPP19. *Nature* 625: 195–203

Pomerening JR, Sontag ED & Ferrell JE (2003) Building a cell cycle oscillator: hysteresis and bistability in the activation of Cdc2. *Nat Cell Biol* 5: 346–351

Sha W, Moore J, Chen K, Lassaletta AD, Yi C-S, Tyson JJ & Sible JC (2003) Hysteresis drives cell-cycle transitions in *Xenopus* laevis egg extracts. *Proceedings of the National Academy of Sciences* 100: 975–980

Sieburth DS, Sundaram M, Howard RM & Han M (1999) A PP2A regulatory subunit positively regulates Ras-mediated signaling during Caenorhabditis elegans vulval induction.

Genes Dev 13: 2562–2569

Stiernagle T (2006) Maintenance of C. elegans. *WormBook*: 1–11

Vigneron S, Brioudes E, Burgess A, Labbe JC, Lorca T & Castro A (2009) Greatwall maintains mitosis through regulation of PP2A. *EMBO J* 28: 2786–93

Vigneron S, Gharbi-Ayachi A, Raymond A-A, Burgess A, Labbe J-C, Labesse G, Monsarrat B, Lorca T & Castro A (2011) Characterization of the Mechanisms Controlling Greatwall Activity. *Molecular and Cellular Biology* 31: 2262–2275

Vigneron S, Sundermann L, Labbé J-C, Pintard L, Radulescu O, Castro A & Lorca T (2018) Cyclin A-cdk1-Dependent Phosphorylation of Bora Is the Triggering Factor Promoting Mitotic Entry. *Dev Cell* 45: 637-650.e7

Williams BC, Filter JJ, Blake-Hodek KA, Wadzinski BE, Fuda NJ, Shalloway D & Goldberg ML (2014) Greatwall-phosphorylated Endosulfine is both an inhibitor and a substrate of PP2A-B55 heterotrimers. *eLife* 3: e01695

FIGURE LEGENDS

Figure 1. PP2A-B55 inhibition by FAM122A does not involve changes in PP2A-C or Wee1 levels. (a) 20 µl of interphase extracts were supplemented with a final concentration of 7.15 µM of *Xenopus* or of human FAM122A and 0,8 µl of the mix was recovered at different time points to measure the indicated proteins by western blot. **(b)** Arpp19 or PRC1 proteins *"in vitro"* phosphorylated by PKA or by cyclin A/Cdk1 respectively were supplemented at a final concentration of 1.65 µM together with *Xenopus* or human FAM122A (final concentration of 14.3 µM) to kinase inactivated interphase extracts and the dephosphorylation rate of S113 of Arpp19 and T481 of PRC1 as well as the levels of *Xenopus* and human FAM122A were analysed by western blot. **(c)** Interphase extracts were supplemented (Xe/HuFAM-PD) or not (CT-PD) with either *Xenopus* or human FAM122A as in (a) and used for histidine pull-down. The levels of PP2A B55, A and C subunits as well as the amount of FAM122A were checked by western blot.

Figure 2. FAM122A triggers mitotic entry by inhibiting PP2A-B55 and permitting cyclin A/Cdk-dependent phosphorylation of mitotic substrates. (a) Extracts were treated as for Figure 1a and the levels of the indicated proteins as well as the phosphorylation of Cdk1 on tyrosine 15 were checked by western blot. **(b)** His-wildtype Arpp19, the Gwl phosphorylation site mutant (Serine 71 -to-Alanine) of this protein, His-human FAM122A and His-*Xenopus*

FAM122A were phosphorylated "*in vitro*" by GST-human GwlK72M hyperactive mutant in a final phosphorylation reaction mixture of 10 µl. 5 µl were then used for western blot using anti-histidine antibodies to detect Arpp19 and human and *Xenopus* FAM122A levels or anti-Gwl antibodies to detect Gwl amount. The rest was used to detect γ^{33}P by autoradiography. **(c)** Interphase extracts were depleted with a control or anti-Gwl antibodies and supplemented with Xe FAM122A. Samples were then analysed over time for the levels and phosphorylation of the indicated proteins. **(d)** Interphase extracts were supplemented with the *Xenopus* FAM122A protein in which all serine/threonine residues were mutated into alanine. Samples were recovered at the indicated time points and used for western blot. **(e)** Interphase extracts supplemented with a wildtype or a *Xenopus* FAM122A protein in which all serine/threonine residues were mutated into alanine and used for histidine pulldown and western blot to measure their association with B55, A and C subunits of PP2A. **(f)** Interphase extracts were depleted using control or anti-Cdc25 antibodies, or submitted to two consecutive depletions using firstly anti-Cdc25 and secondly anti-cyclin A antibodies. Depleted supernatants were then supplemented with Xe FAM122A protein. When indicated, purified cyclin A was added to the mix to a final concentration of 100 nM. Samples were recovered over time and used for western blot. Depletion of cyclin A and Cdc25 in the extracts was confirmed by western blot.

Figure 3. Molecular determinants controlling FAM122A inhibitory activity. (a) AlphaFold Monomer v2.0 predicts two structured αhelices (αHelix 1 and αHelix 2) in the human FAM122A protein and human. *Xenopus laevis* amino acid sequence alignment. αHelix 1 and αHelix 2 are indicated. **(b)** Interphase extracts were supplemented with the wildtype or the αH1 or αH2 mutants of Xe FAM122A and the phosphorylation and levels of the indicated proteins measured at the indicated times. **(c)** Interphase extracts supplemented with wildtype and αH1 or αH2 mutants were used for His-pulldown to measure the association of these proteins to B55 and C subunits of PP2A-B55. **(d)** The wildtype and the indicated mutant forms of Xe FAM122A were supplemented to interphase extracts and used for western blot. **(e)** His-pulldown was performed in extracts treated as in (d) to check the binding of the different forms of Xe FAM122A form to B55 and C. **(f)** Table indicating the capacity of the different single mutants of Xe FAM122A to induce mitotic entry and to bind to PP2A-B55. Mutants that have lost their inhibitory activity are depicted in red. The sequence of the αH1, the SLiM consensus sequence and the sequence of αH2 are shown. Residues essential to keep the inhibitory activity of Xe FAM122A are highlighted in red.

Figure 4. Gwl activation at mitotic entry promotes the dissociation of FAM122A from PP2A-B55. (a) Interphase and CSF extracts were supplemented with Xe FAM122A and Hu FAM122A and used for His-pulldown to measure the association of this protein with B55 and C subunits of PP2A-B55. The levels of His-Xe/HuFAM122A recovered in the pull down are also shown. Inter PD: Interphase Pull Down. CSF PD: CSF pull down. **(b)** Interphase extracts were depleted with control or with anti-Cdc27 antibodies and subsequently supplemented with Xe FAM122A and used for western blot or for His-pulldown to assess the binding of Xe FAM122A to PP2A-B55. **(c)** Interphase extracts were depleted of Cdc27, submitted to a second immunodepletion using control (lanes 1 & 3) or anti-Gwl antibodies (lanes 2 & 4) and supplemented with Xe FAM122A. 20 minutes later Gwl activity was restored (lanes 3 & 4) or not (lanes 1 & 2) by adding a hyperactive form of Gwl (GwlK72M). Samples were used for western blot and His-pulldown.

Figure 5. Arpp19 dissociates FAM122A from PP2A-B55 during mitosis. (a) Interphase extracts were supplemented with a final concentration of 7.15 μM of Xe FAM122A and 40 minutes later divided into two samples. One of these samples was used to perform a His-pulldown that was then supplemented with a final concentration of 2.7 μM of untagged Thio-Arpp19 protein and used to measure bound B55 protein. The second sample was firstly supplemented with untagged 69.3 pmol of Thio-Arpp19 and subsequently used for His-pulldown to measure His-Xe FAM122A bound B55 subunit of PP2A. A sample of the His-Xe FAM122A pull downs supplemented (PD+Arp) or not (PD-Arp) with untagged Thio-Arpp19 is shown. **(b)** CSF extracts were supplemented with a final concentration of 3,6 μM His-Arpp19 and, 40 minutes later, used for His-pulldown. Arpp19-pull downs were then supplemented with a final concentration of 10 μM GST-Xe FAM122A and the levels of B55 remaining were measured. A sample of the His-Arpp19 pull downs supplemented (PD+FAM) or not (PD-FAM) is shown. **(c)** Table indicating the kinetic parameters of the dephosphorylation of the PP2A-B55 substrate p-S113-Arpp19 and the inhibitory constant of FAM122A and Thio-S71-Arpp19 in kinase inactivated interphase extracts. Conditions used in these assays are detailed in Methods. **(d)** Interphase extracts were supplemented with His-Xe FAM122A and used for either western blot to measure the levels and the phosphorylation of the indicated proteins and or for His-pulldown determine Xe FAM122A binding to PP2A B55, A and C subunits at the indicated time points. **(e)** Interphase extracts were supplemented with His-FAM122A to the indicated final concentrations and mitotic entry was assessed by

the phosphorylation of Gwl, dephosphorylation of tyrosine 15 of Cdk1 and the degradation of cyclin B2.

Figure 6. Arpp19 and FAM122A differently bind PP2A-B55. **(a)** Superposition of the models of Arpp19/ENSA and FAM122A in complex with ternary PP2A-B55 as predicted by Alphafold_multimer v 2.2 for three species (human, *Xenopus* and *C. elegans*). Arrp19/ENSA and truncated FAM122A are in orange ribbon while PP2A-B55 is in blue (B55), dark green (catalytic C subunit) and pink (the scaffold A subunit). **(b)** Zoom onto the entrance of the catalytic site of PP2A in complex with human Arpp19 and FAM122A. Manganese ions are shown as black spheres and sidechains are drawn as sticks with carbon colours as the corresponding polypeptide chains. Figure was drawn using Pymol (http://www.pymol.org).

Figure 7. FAM122A is required to correctly enter into mitosis in *C elegans*. (a) Arpp19 or PRC1 *"in vitro"* phosphorylated by PKA or Cdk1 respectively were supplemented together with Ce FAM122A to interphase extracts and the levels and dephosphorylation rate of S113 of Arpp19 or T481 of PRC1, as well as the amount of Ce FAM122A, were analysed by western blot. **(b)** Ce FAM122A was added to interphase extracts and the levels and phosphorylation of the indicated proteins measured by western blot. **(c)** Scheme representing the genetic dependences of the gain of function *let-60(gf)* mutant and *sur-6* (B55 orthologue) mutant on multivulva phenotype in *C. elegans*. *sur-6* mutant (diminishes PP2A-B55 activity) on a *let-60(gf)* mutant background decreases the multivulva phenotype. Conversely, the depletion of *F46H5.2* (FAM122A orthologue) in a *let-60(gf)* mutant background significantly increases this phenotype suggesting that, as expected, *F46H5.2* protein would act as an inhibitor of PP2A-B55 in *C. elegans*. Big red arrows: increased multivulva phenotype. Shown are two representative images of a wildtype worm displaying one vulva or a mutant worm with a multivulva phenotype. The percentage of worms displaying multivulva phenotype in each mutant is represented as a mean+/- standard deviation. Significant differences calculated by non-parametric two tailed Mann-Whitney test are shown. **(d)** The number of larvae, dead embryos and unfertilized eggs were counted for control and *F46H5.2(RNAi)* worms and represented as mean values +/- standard deviation. **(e)** The percentage of dead embryos and unfertilized eggs were counted in worms at first day of adulthood and represented as for (d).

Figure 8. FAM122A is required *"in vivo"* in *C. elegans* to permit mitotic entry and progression in germ stem cells. (a) Nematode strains expressing histone and gamma-tubulin

tagged with GFP were immobilised and immediately imaged by confocal microscopy for the quantification of interphase and mitotic cells as reported in the scheme of Appendix Figure S6. Data are represented as mean ± standard deviation. **(b)** Prophase, metaphase and anaphase germ stem cells in gonads of worms were counted as in (a) and represented as mean ± standard deviation. **(c)** A GFP-tagged tubulin and with RFP-tagged histone nematode strain was followed by time lapse confocal microscopy and the timing of mitotic progression was determined in germ stem cells. Shown are representative images of stem cells performing mitotic division over time in control and RNAi treated worms. The number of cells performing nuclear envelope breakdown (NEBD) per minute and per gonad were counted and represented as the mean values ± standard deviation. Timing of cells to perform prophase (from first centrosome movement to nuclear envelope breakdown), congression (from nuclear envelope breakdown to metaphase plate) or anaphase onset were also recorded and represented as mean values ± standard deviation. Significant differences calculated by non-parametric two tailed Mann-Whitney test are shown. Arrowheads: centrosomes. P:prophase. Sp: Spermatozoids. PM: prometaphase. A: anaphase. Scale bar: 10 μm. * $p<0.01$; *** $p<0.001$; **** $p<0.0001$. $n\geq10$. **(d)** RPE1 cells were (Thymidine Block) or not (Asynchronous) synchronized with thymidine treatment and released at the indicated timepoints. Released cells were used for western blot to measure FAM122A, cyclin A and tubulin levels at the different timepoints. Western blot signals were measured and FAM122A and cyclin A amounts were normalized and represented. n=2.

Figure 9. Hypothetic model representing the network of activation/inactivation of cyclin B/Cdk1 and mitotic entry/exit by the sequential inhibition of PP2A-B55 by FAM122A and Arpp19. PP2A-B55 activity is maintained high during G2 preventing the phosphorylation and activation of Cdc25 by cyclin A/Cdk. A first phosphorylation and activation of Cdc25 phosphatase by cyclin A/Cdk is achieved when a critical FAM122A-dependent inhibition of PP2A-B55 is reached. Cdc25 will then dephosphorylate and activate the cyclin B/Cdk1 feedback loop resulting in the activation of Gwl, phosphorylation of Arpp19 and mitotic entry. Phospho-Arpp19 will then induce FAM122A dissociation of PP2A-B55 taking over the inhibition of this phosphatase and promoting the correct temporal dephosphorylation of mitotic substrates. Active and inactive pathways are represented as solid thick arrows and dashed thin arrows respectively. Activatory phosphorylation sites are represented in red whereas inhibitory phosphorylation of Cdk1 is shown in blue.

1094

1095

1096

Figure 1

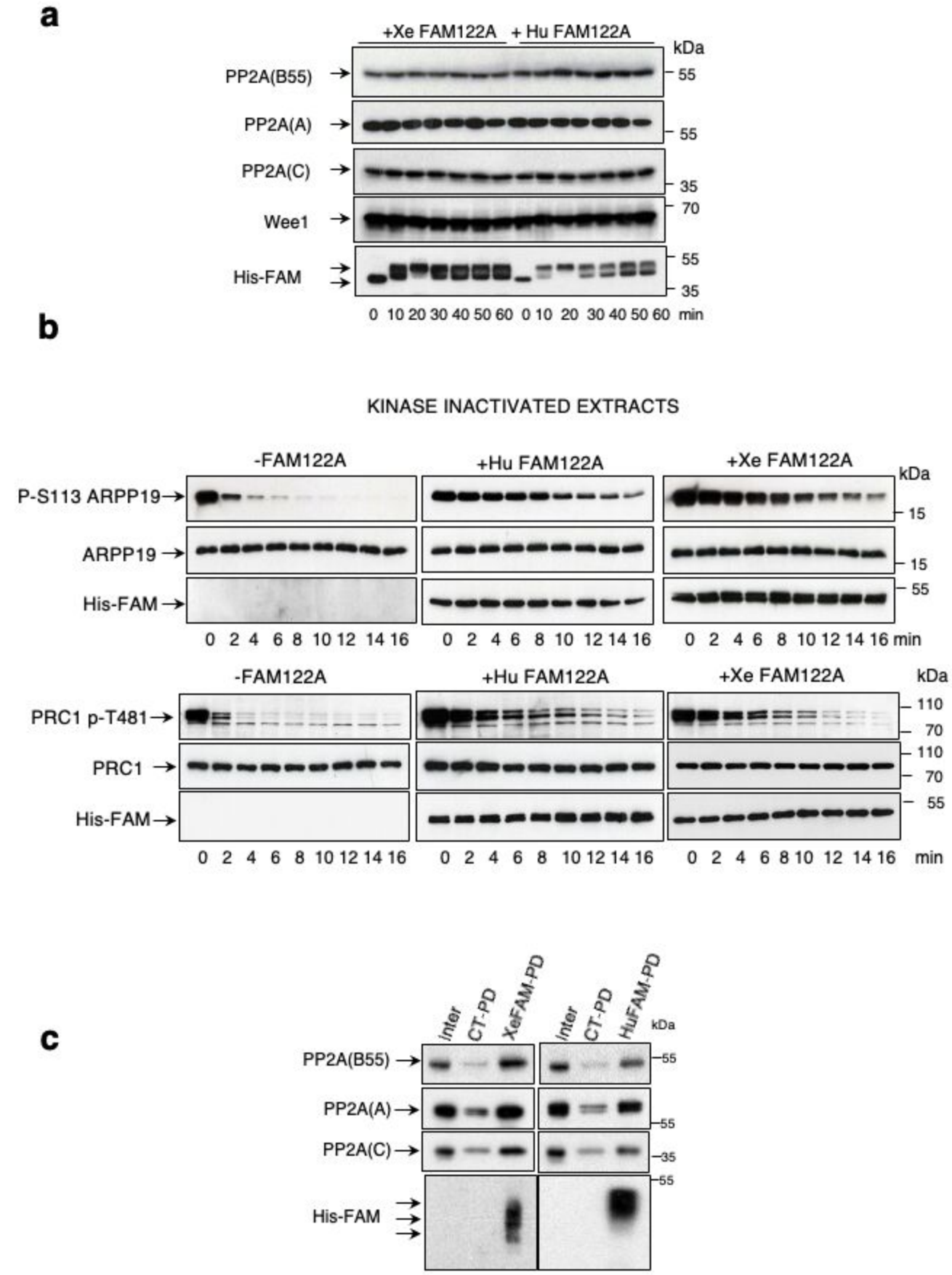
a
+Xe FAM122A
+ Hu FAM122A
kDa
PP2A(B55)
PP2A(A)
PP2A(C)
Wee1
His-FAM
55
55
35
70
55
35
0 10 20 30 40 50 60 0 10 20 30 40 50 60 min
b
KINASE INACTIVATED EXTRACTS
-FAM122A
+Hu FAM122A
+Xe FAM122A
kDa
P-S113 ARPP19
ARPP19
His-FAM
15
15
55
0 2 4 6 8 10 12 14 16 0 2 4 6 8 10 12 14 16 0 2 4 6 8 10 12 14 16 min
-FAM122A
+Hu FAM122A
+Xe FAM122A
kDa
PRC1 p-T481
PRC1
His-FAM
110
70
110
70
55
0 2 4 6 8 10 12 14 16 0 2 4 6 8 10 12 14 16 0 2 4 6 8 10 12 14 16 min
c
inter
CT-PD
XeFAM-PD
inter
CT-PD
HuFAM-PD
kDa
PP2A(B55)
PP2A(A)
PP2A(C)
His-FAM
55
55
35
55

Figure 2

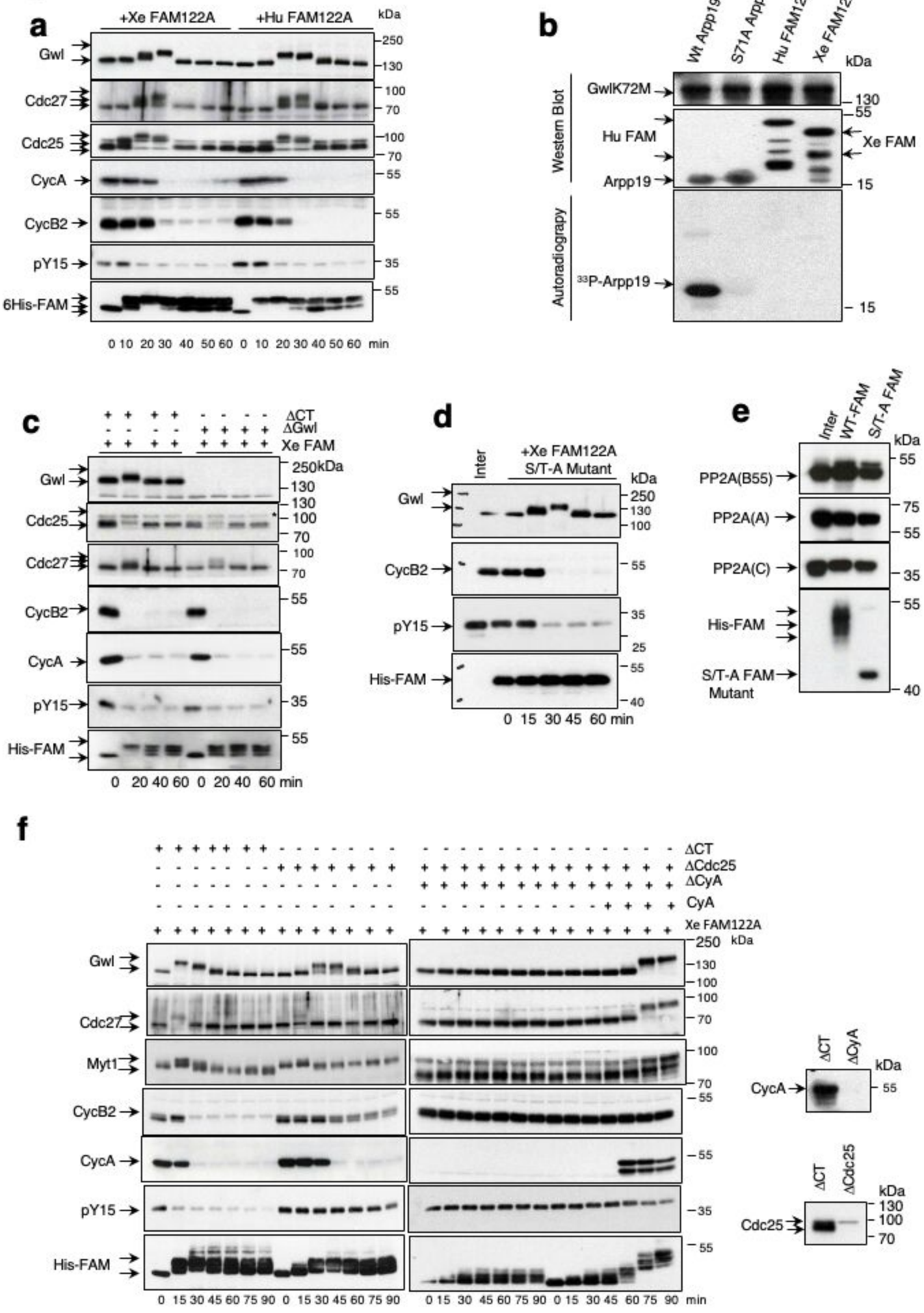
a
+Xe FAM122A
+Hu FAM122A
kDa
Gwl
Cdc27
Cdc25
CycA
CycB2
pY15
6His-FAM
0 10 20 30 40 50 60 0 10 20 30 40 50 60 min
b
Wt Arpp19
S71A Arpp19
Hu FAM122A
Xe FAM122A
kDa
Western Blot
GwlK72M
Hu FAM
Xe FAM
Arpp19
Autoradiography
33P-Arpp19
c
ΔCT
ΔGwl
Xe FAM
250kDa
Gwl
Cdc25
Cdc27
CycB2
CycA
pY15
His-FAM
0 20 40 60 0 20 40 60 min
d
Inter
+Xe FAM122A S/T-A Mutant
kDa
Gwl
CycB2
pY15
His-FAM
0 15 30 45 60 min
e
Inter
WT-FAM
S/T-A FAM
kDa
PP2A(B55)
PP2A(A)
PP2A(C)
His-FAM
S/T-A FAM Mutant
f
ΔCT
ΔCdc25
ΔCyA
CyA
Xe FAM122A
kDa
Gwl
Cdc27
Myt1
CycB2
CycA
pY15
His-FAM
0 15 30 45 60 75 90 0 15 30 45 60 75 90
0 15 30 45 60 75 90 0 15 30 45 60 75 90 min
ΔCT
ΔCyA
kDa
CycA
ΔCT
ΔCdc25
kDa
Cdc25

Figure 3

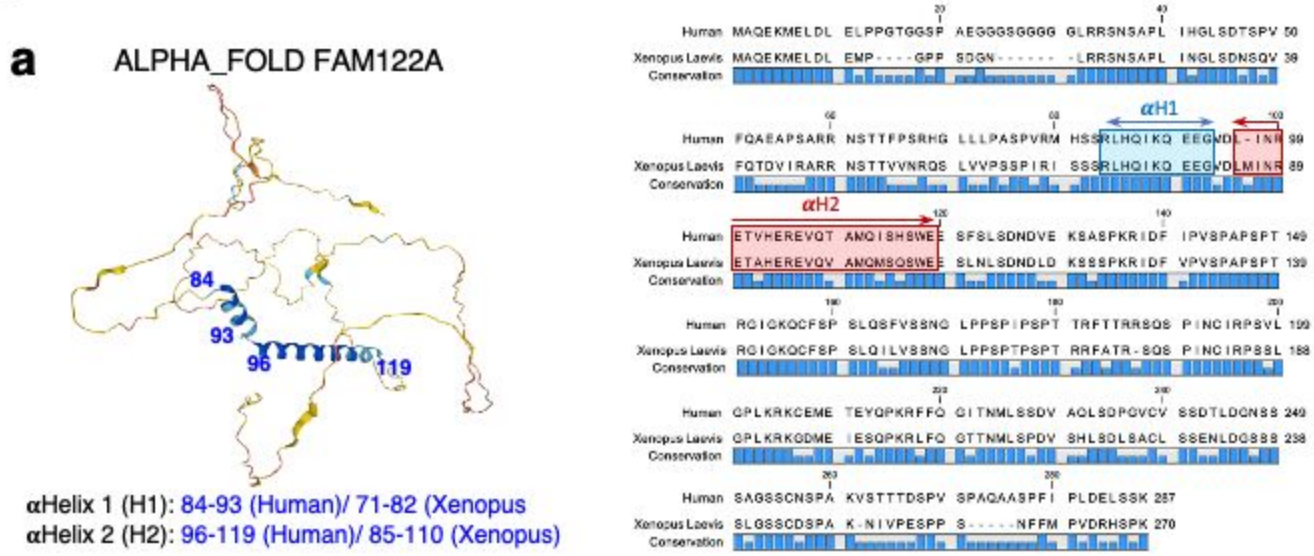

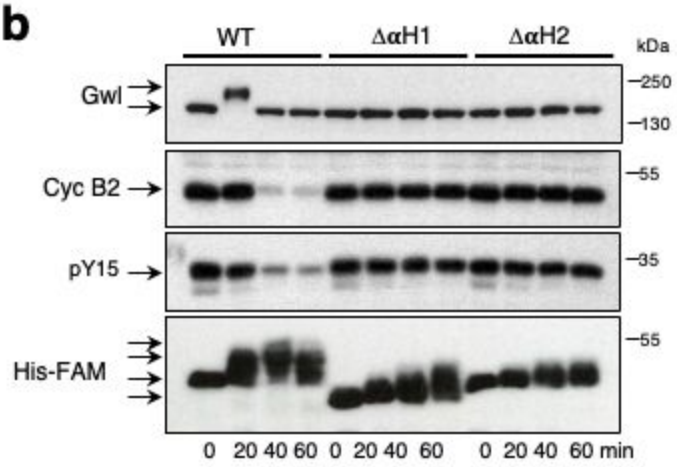

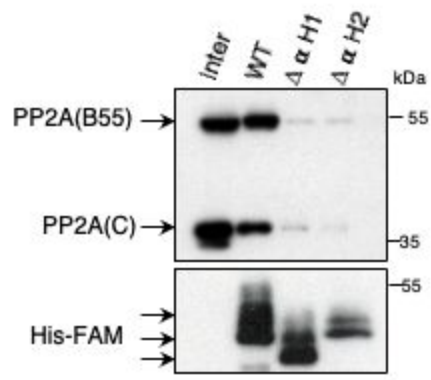

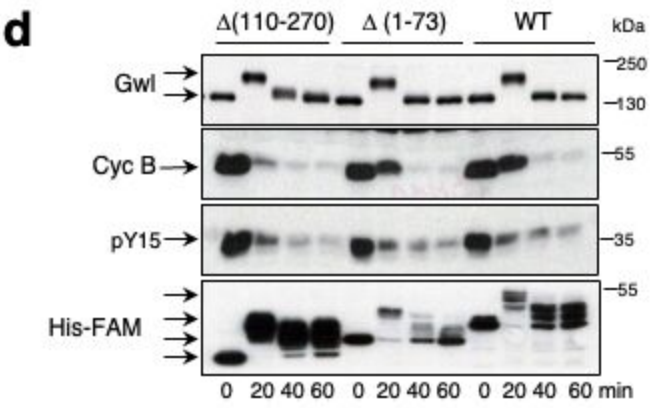

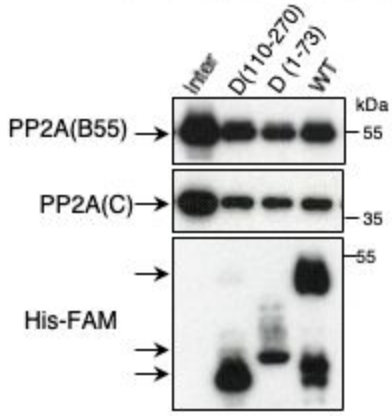

f

	Mutants Xenopus	Mitotic Entry	PP2A Binding
H1	R73A	-	-
	L74N	-	-
	I77N	-	-
	K78R	+	+
	E80A	-	-
H2	L85N	+	+
	I87N	+	+
	E90A	-	-
	H93A	-	-
	E94A	-	-
	R95A	-	-
	S104A	+	+
	E108A	+	+
	E109A	+	+

αH1: SRLHQIKQEE **SLiM Consensus:** [RK]-V-xx-[VI]-R

αH2: DLMINRETAHEREVQVAMQMSQSWSEE

Figure 4

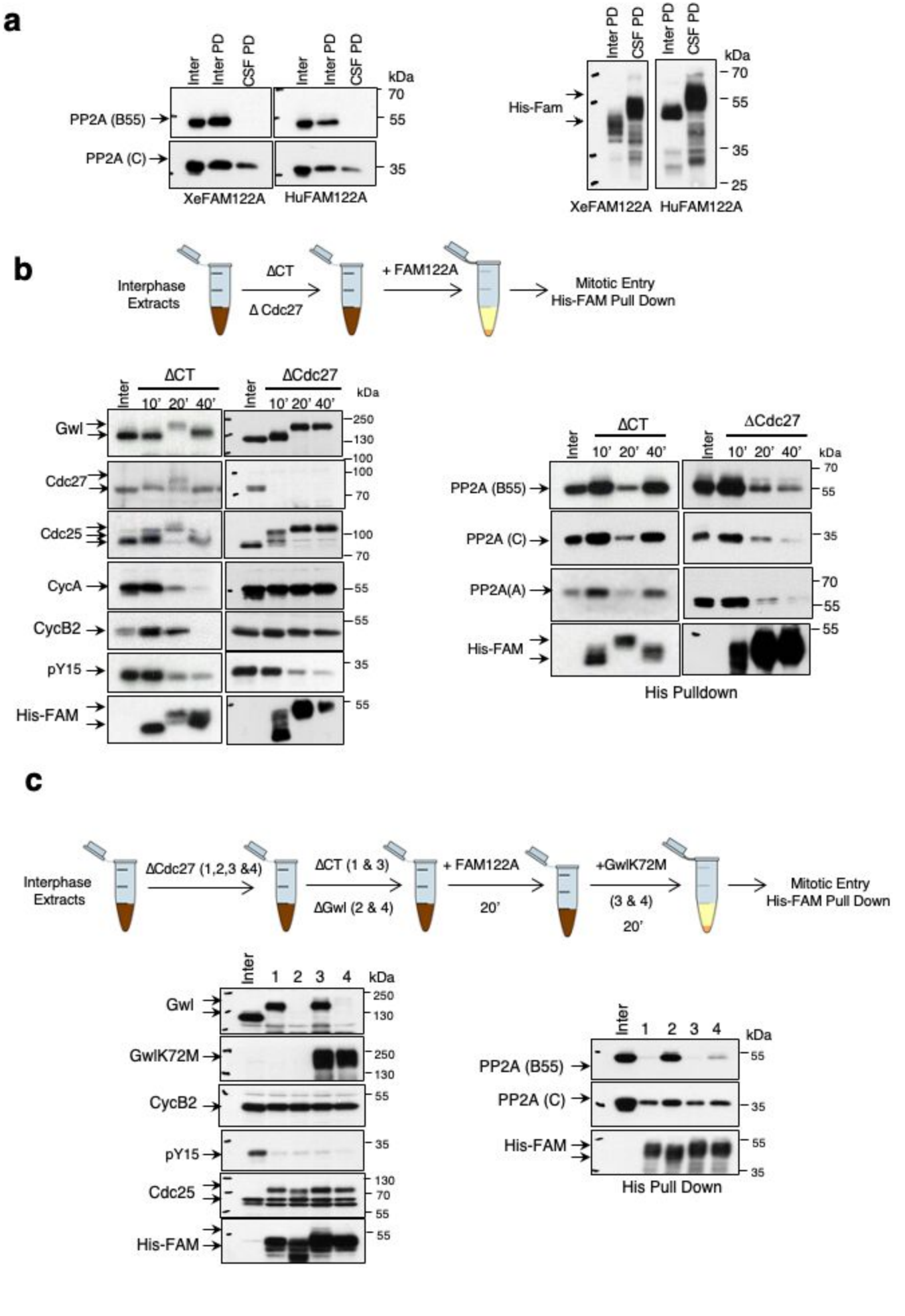
a
Inter
Inter PD
CSF PD
kDa
70
55
35
PP2A (B55)
PP2A (C)
XeFAM122A
HuFAM122A
His-Fam
25
b
Interphase Extracts
ΔCT
Δ Cdc27
+ FAM122A
Mitotic Entry
His-FAM Pull Down
10' 20' 40'
Gwl
Cdc27
Cdc25
CycA
CycB2
pY15
His-FAM
250
130
100
PP2A(A)
His Pulldown
c
ΔCdc27 (1,2,3 &4)
ΔCT (1 & 3)
ΔGwl (2 & 4)
20'
+GwlK72M
(3 & 4)
1 2 3 4
GwlK72M
His Pull Down

Figure 5

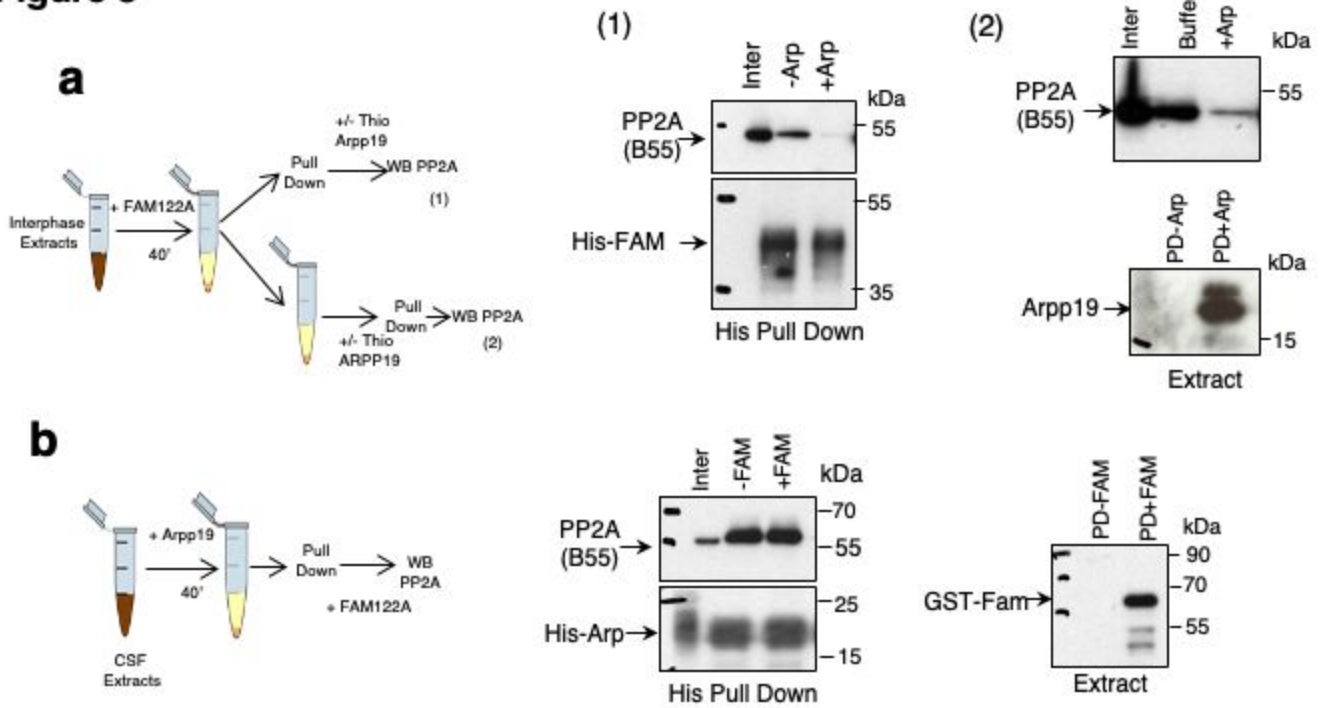

c

	V_{max} (nM)	K_m (nM)	K_i (nM)
pS113-Arpp19	89±3.5	146±23.9	
pS67-Arpp19			0.22±0.04
FAM122A			28±4.6

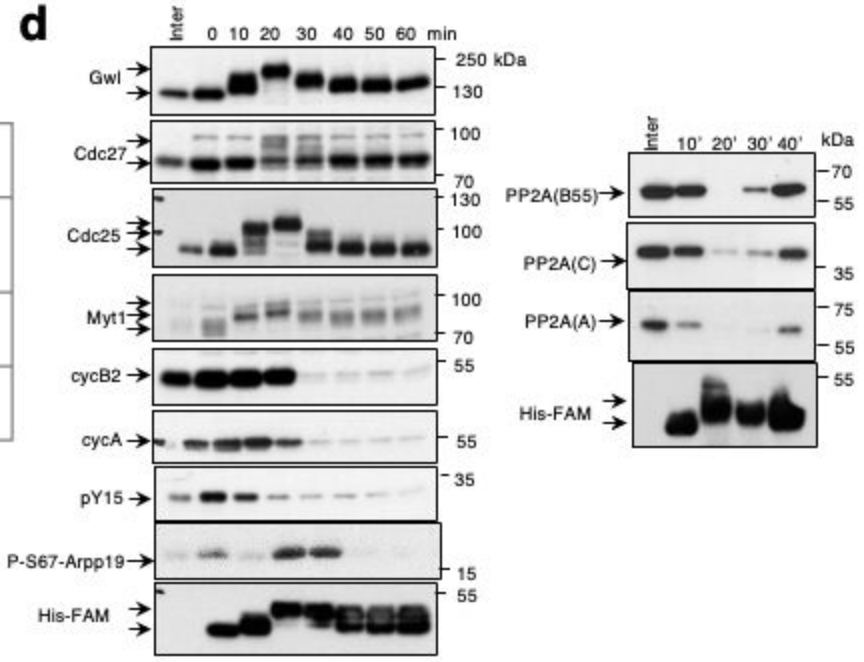

e

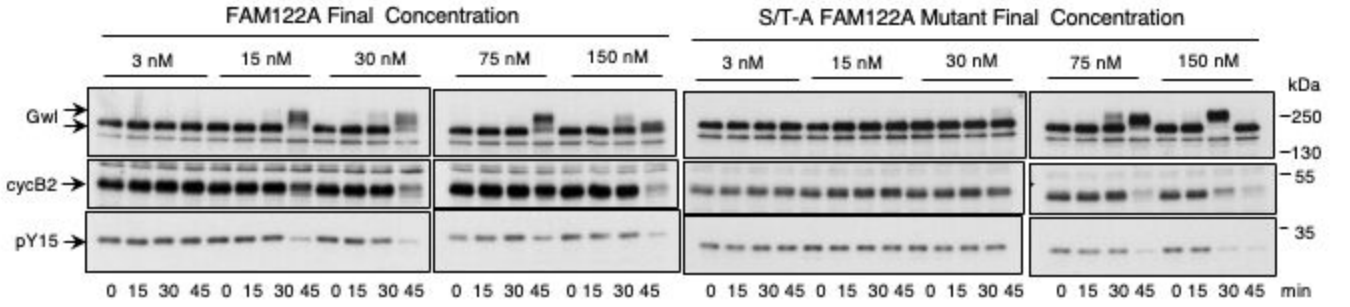

Figure 6

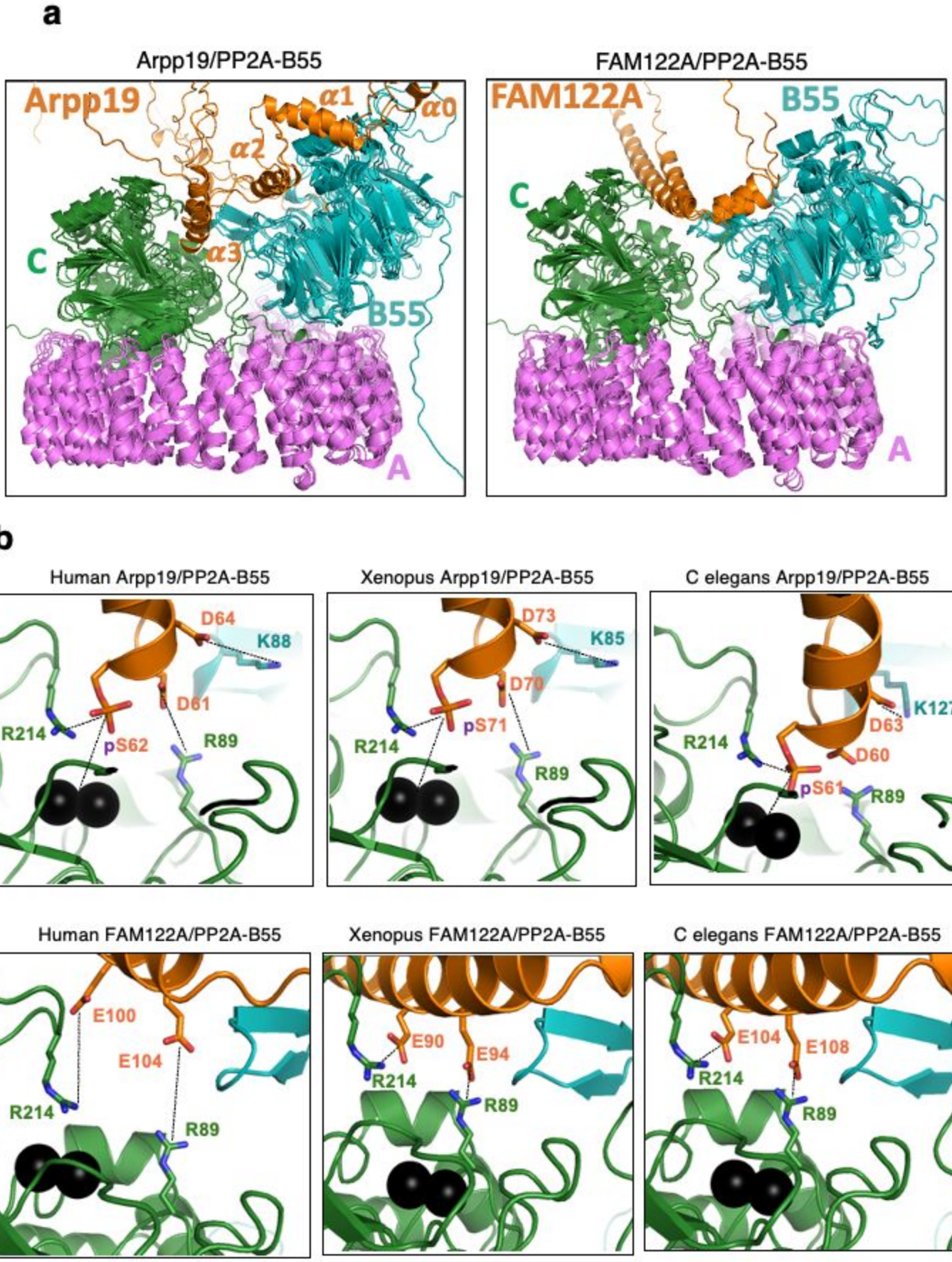
a
Arpp19/PP2A-B55
FAM122A/PP2A-B55
Arpp19
α1
α0
α2
α3
C
B55
A
FAM122A
B55
C
A
b
Human Arpp19/PP2A-B55
D64
K88
D61
R214
pS62
R89
Xenopus Arpp19/PP2A-B55
D73
K85
D70
pS71
R214
R89
C elegans Arpp19/PP2A-B55
K127
D63
R214
D60
pS61
R89
Human FAM122A/PP2A-B55
E100
E104
R214
R89
Xenopus FAM122A/PP2A-B55
E90
E94
R214
R89
C elegans FAM122A/PP2A-B55
E104
E108
R214
R89

Figure 7

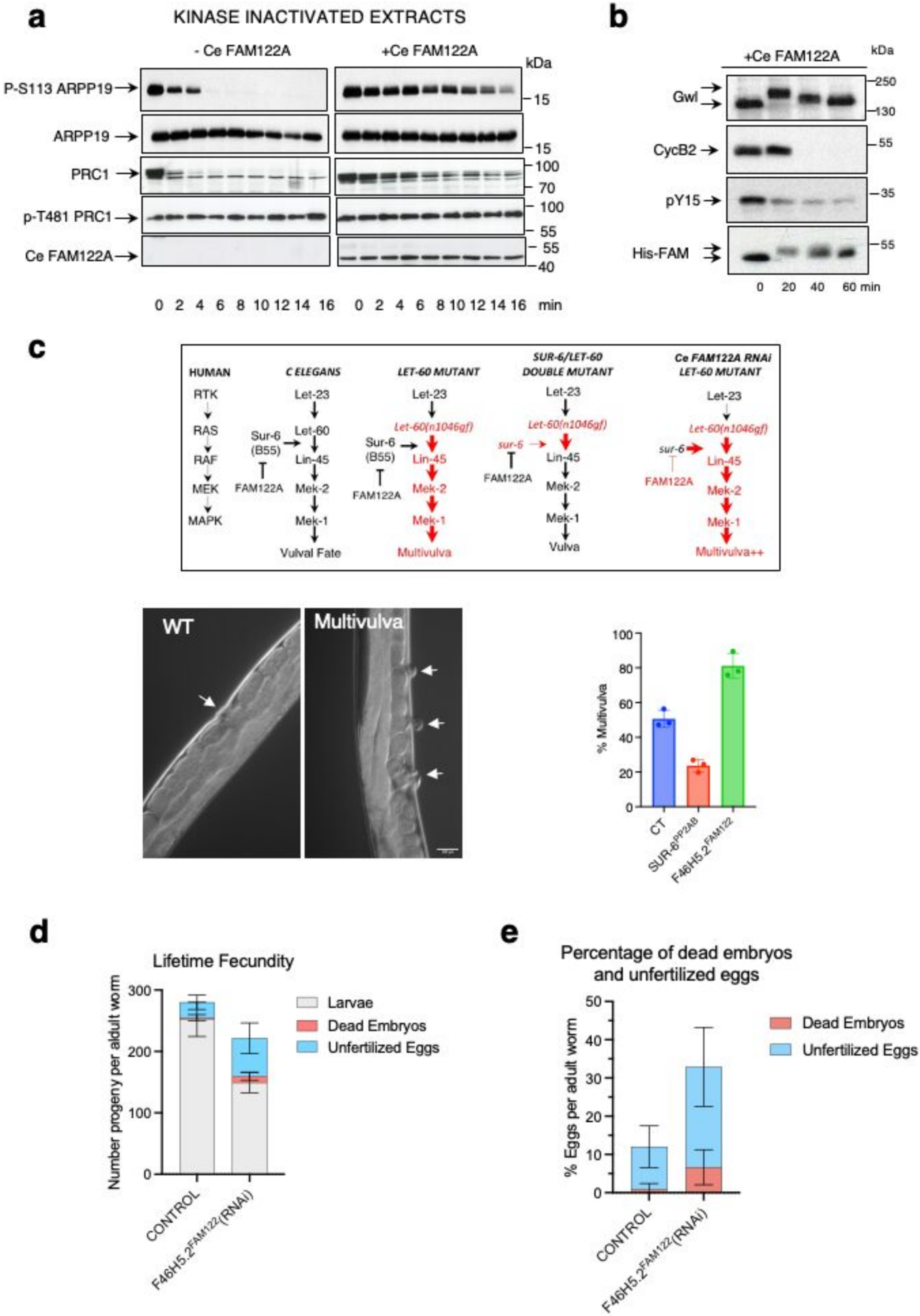
a
KINASE INACTIVATED EXTRACTS
- Ce FAM122A
+Ce FAM122A
kDa
P-S113 ARPP19
ARPP19
PRC1
p-T481 PRC1
Ce FAM122A
15
15
100
70
100
55
55
40
0 2 4 6 8 10 12 14 16 0 2 4 6 8 10 12 14 16 min
b
+Ce FAM122A
kDa
Gwl
CycB2
pY15
His-FAM
250
130
55
35
55
0 20 40 60 min
c
HUMAN
RTK
RAS
RAF
MEK
MAPK
C ELEGANS
Let-23
Let-60
Lin-45
Mek-2
Mek-1
Vulval Fate
Sur-6 (B55)
FAM122A
LET-60 MUTANT
Let-60(n1046gf)
Multivulva
SUR-6/LET-60 DOUBLE MUTANT
sur-6
Vulva
Ce FAM122A RNAi LET-60 MUTANT
Multivulva++
WT
Multivulva
% Multivulva
CT
SUR-6PP2AB
F46H5.2FAM122
d
Lifetime Fecundity
Number progeny per adult worm
Larvae
Dead Embryos
Unfertilized Eggs
CONTROL
F46H5.2FAM122(RNAi)
e
Percentage of dead embryos and unfertilized eggs
% Eggs per adult worm
Dead Embryos
Unfertilized Eggs
CONTROL
F46H5.2FAM122(RNAi)

Figure 8

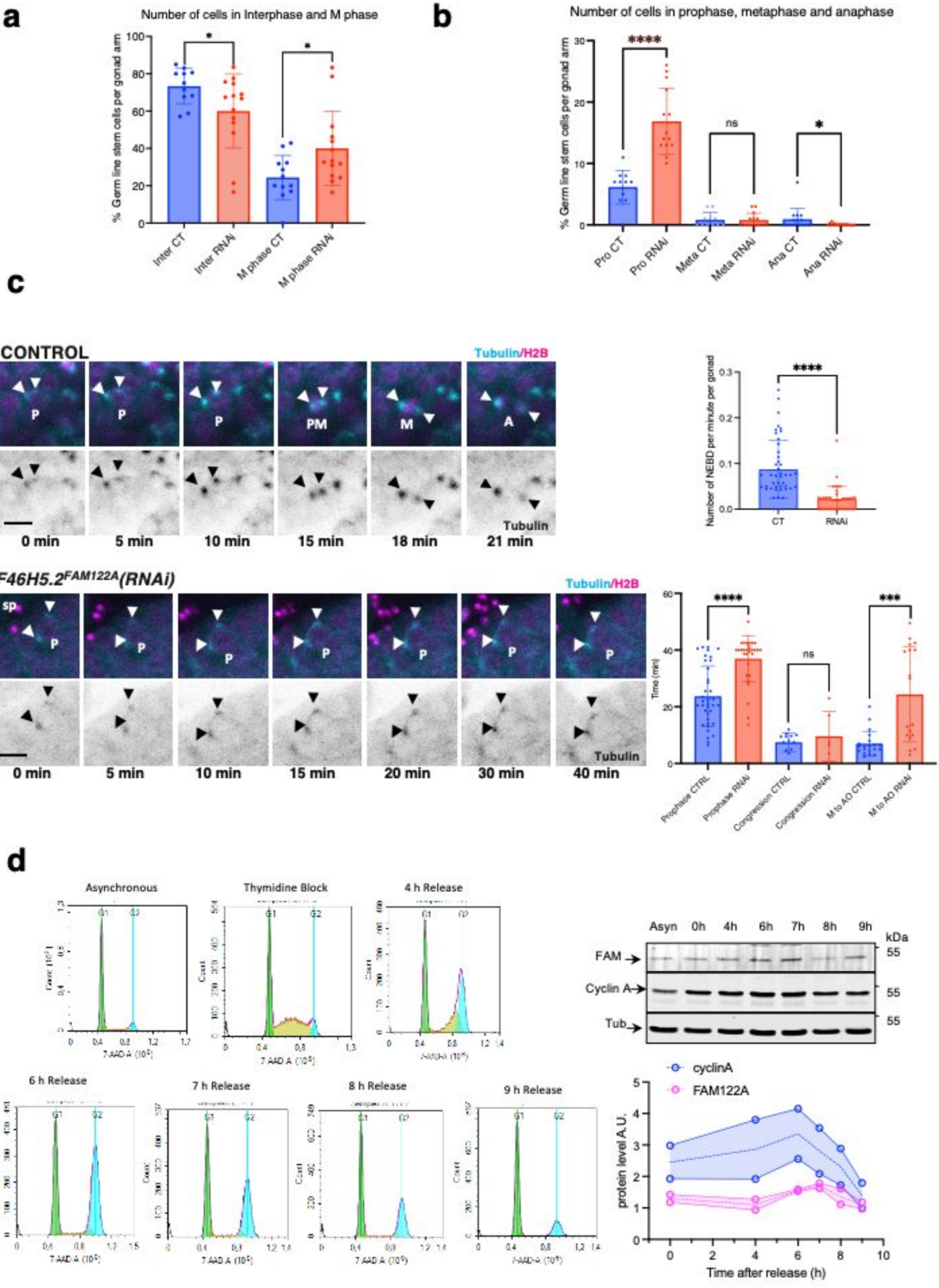
a
Number of cells in Interphase and M phase
% Germ line stem cells per gonad arm
Inter CT
Inter RNAi
M phase CT
M phase RNAi
b
Number of cells in prophase, metaphase and anaphase
% Germ line stem cells per gonad arm
Pro CT
Pro RNAi
Meta CT
Meta RNAi
Ana CT
Ana RNAi
c
CONTROL
Tubulin/H2B
P
PM
M
A
Tubulin
0 min
5 min
10 min
15 min
18 min
21 min
Number of NEBD per minute per gonad
CT
RNAi
F46H5.2FAM122A(RNAi)
Tubulin/H2B
sp
P
Tubulin
0 min
5 min
10 min
15 min
20 min
30 min
40 min
Time (min)
Prophase CTRL
Prophase RNAi
Congression CTRL
Congression RNAi
M to AO CTRL
M to AO RNAi
d
Asynchronous
Thymidine Block
4 h Release
6 h Release
7 h Release
8 h Release
9 h Release
7-AAD-A (10^3)
Asyn
0h
4h
6h
7h
8h
9h
kDa
FAM
Cyclin A
Tub
55
cyclinA
FAM122A
protein level A.U.
Time after release (h)

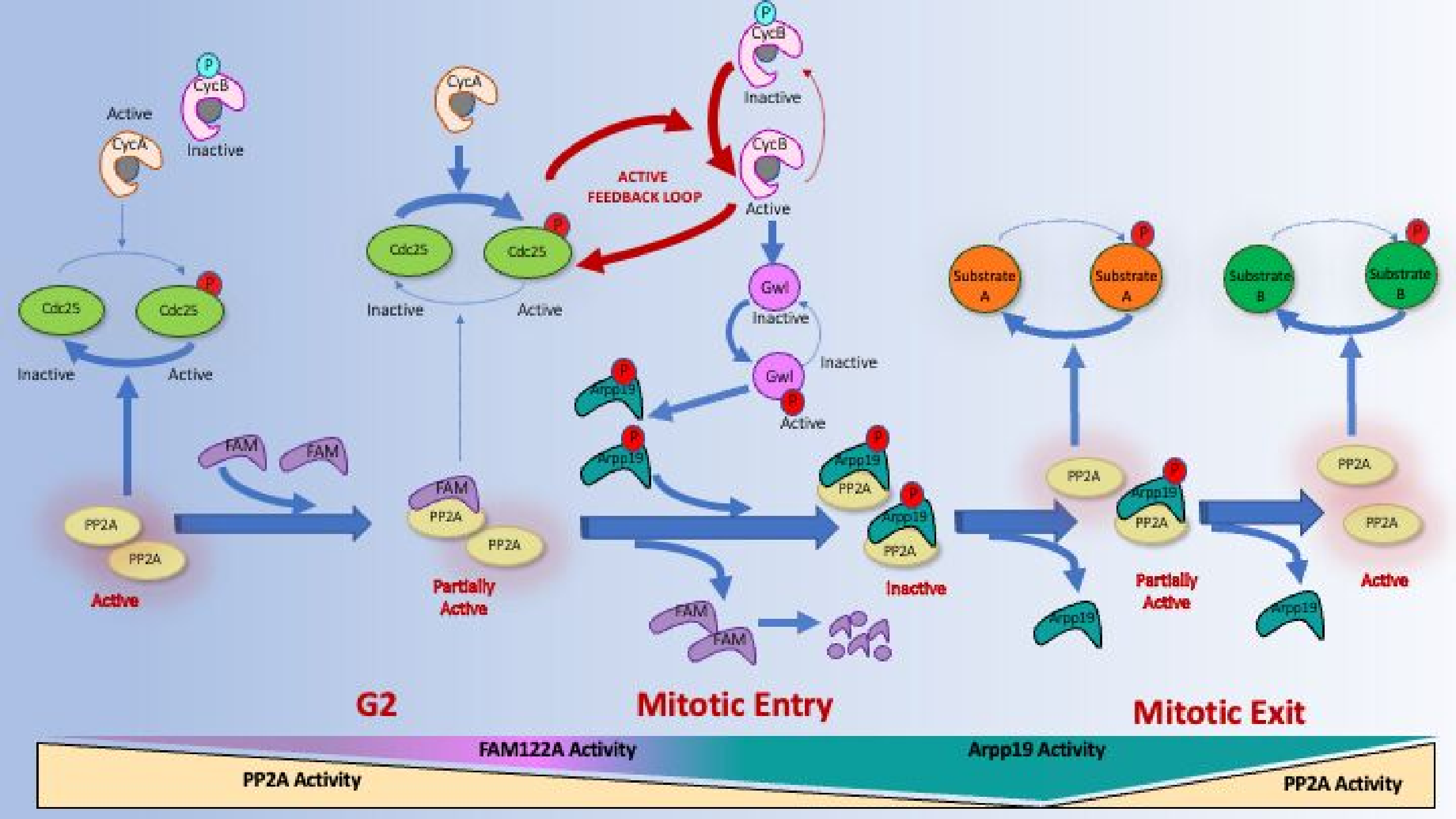
Active
CycA
CycB
Inactive
Cdc25
Cdc25
Inactive
Active
CycA
Cdc25
Cdc25
Inactive
Active
ACTIVE
FEEDBACK LOOP
CycB
Inactive
CycB
Active
Gwl
Inactive
Gwl
Inactive
Active
Substrate A
Substrate A
Substrate B
Substrate B
Arpp19
Arpp19
Arpp19
Arpp19
FAM
FAM
FAM
FAM
PP2A
PP2A
PP2A
PP2A
PP2A
PP2A
PP2A
PP2A
Active
Partially Active
Inactive
Partially Active
Active
G2
Mitotic Entry
Mitotic Exit
FAM122A Activity
PP2A Activity
Arpp19 Activity
PP2A Activity